

BAYESIAN INFERENCE OF HIGH-DENSITY NUCLEAR SYMMETRY ENERGY FROM RADII OF CANONICAL NEUTRON STARS

WEN-JIE XIE^{1,2} AND BAO-AN LI^{1*}

¹Department of Physics and Astronomy, Texas A&M University-Commerce, Commerce, TX 75429, USA

²Department of Physics, Yuncheng University, Yuncheng 044000, China

*Corresponding author: Bao-An.Li@Tamuc.edu

ABSTRACT

The radius $R_{1.4}$ of neutron stars (NSs) with a mass of $1.4 M_{\odot}$ has been extracted consistently in many recent studies in the literature. Using representative $R_{1.4}$ data, we infer high-density nuclear symmetry energy $E_{\text{sym}}(\rho)$ and the associated nucleon specific energy $E_0(\rho)$ in symmetric nuclear matter (SNM) within a Bayesian statistical approach using an explicitly isospin-dependent parametric Equation of State (EOS) for nucleonic matter. We found that: (1) The available astrophysical data can already improve significantly our current knowledge about the EOS in the density range of $\rho_0 - 2.5\rho_0$. In particular, the symmetry energy at twice the saturation density ρ_0 of nuclear matter is determined to be $E_{\text{sym}}(2\rho_0) = 39.2^{+12.1}_{-8.2}$ MeV at 68% confidence level. (2) A precise measurement of the $R_{1.4}$ alone with a 4% 1σ statistical error but no systematic error will not improve much the constraints on the EOS of dense neutron-rich nucleonic matter compared to what we extracted from using the available radius data. (3) The $R_{1.4}$ radius data and other general conditions, such as the observed NS maximum mass and causality condition introduce strong correlations for the high-order EOS parameters. Consequently, the high-density behavior of $E_{\text{sym}}(\rho)$ inferred depends strongly on how the high-density SNM EOS $E_0(\rho)$ is parameterized, and vice versa. (4) The value of the observed maximum NS mass and whether it is used as a sharp cut-off for the minimum maximum mass or through a Gaussian distribution affect significantly the lower boundaries of both the $E_0(\rho)$ and $E_{\text{sym}}(\rho)$ only at densities higher than about $2.5\rho_0$.

Keywords: Dense matter, equation of state, stars: neutron

1. INTRODUCTION

The energy per nucleon $E(\rho, \delta)$ (also referred as nucleon specific energy) in nuclear matter at nucleon density ρ , isospin asymmetry $\delta \equiv (\rho_n - \rho_p)/\rho$ and zero temperature is the most basic input for calculating the Equation of State (EOS) of cold neutron star (NS) matter regardless of the complexity of the models used. It can be well approximated by the isospin-parabolic expansion (Bombaci & Lombardo 1991)

$$E(\rho, \delta) = E_0(\rho) + E_{\text{sym}}(\rho) \cdot \delta^2 + \mathcal{O}(\delta^4), \quad (1)$$

where $E_0(\rho)$ is the energy per nucleon in symmetric nuclear matter (SNM) having equal numbers of neutrons and protons while the symmetry energy $E_{\text{sym}}(\rho)$ encodes the energy associated with the neutron-richness of the system. On one hand, much progress has been made over the last few decades in constraining the SNM EOS $E_0(\rho)$ not only around but also significantly above the saturation density of nuclear matter $\rho_0 \approx 2.8 \times 10^{14} \text{ g/cm}^3$ (corresponding to $\rho_0 \approx 0.16 \text{ nucleons/fm}^3$) by combining the knowledge gained from analyzing both astrophysical observations and terrestrial nuclear experiments, see, e.g., refs. (Danielewicz et al. 2002; Oertel et al. 2017; Trautmann and Wolter 2017; Garg & Colò 2018; Vidaña 2018; Burgio & Fantina 2018; Zhang & Li 2019c). On the other hand, while the symmetry energy $E_{\text{sym}}(\rho)$ mostly around and below ρ_0 has been relatively well constrained in recent years (Li et al. 2014), very little is known about the symmetry energy at supra-saturation densities. In fact, it has been broadly recognized that the high-density nuclear symmetry energy is presently among the most important but undetermined quantities reflecting the still mysterious nature of dense neutron-rich nuclear matter (Baran et al. 2005; Steiner et al. 2005; Li et al. 2008; Lattimer 2012; Tsang et al. 2012; Horowitz et al. 2014; Baldo & Burgio 2016; Li 2017). Thus not surprisingly, to determine the density dependence of nuclear symmetry energy was identified as a major scientific thrust for nuclear astrophysics in both the U.S. 2015 Long Range Plan for Nuclear Sciences (U.S. LRP 2015) and the Nuclear Physics European Collaboration Committee (NuPECC) 2017 Long Range Plan (NuPECC LRP 2017).

Both the magnitude and slope of nuclear symmetry energy contribute to the pressure of NS matter. For example, the pressure of *npe* matter in NSs at β equilibrium at density ρ and isospin asymmetry δ is explicitly

$$P(\rho, \delta) = \rho^2 \left[\frac{dE_0(\rho)}{d\rho} + \frac{dE_{\text{sym}}(\rho)}{d\rho} \delta^2 \right] + \frac{1}{2} \delta(1 - \delta) \rho \cdot E_{\text{sym}}(\rho). \quad (2)$$

The first term is the SNM pressure $P_0(\rho) = \rho^2 \frac{dE_0(\rho)}{d\rho}$ while the last two terms are the isospin-asymmetric pressure $P_{\text{asy}}(\rho, \delta) = \rho^2 \frac{dE_{\text{sym}}(\rho)}{d\rho} \delta^2 + \frac{1}{2} \delta(1 - \delta) \rho \cdot E_{\text{sym}}(\rho)$ from nucleons and electrons, separately. At the saturation density ρ_0 , the P_0 vanishes and the electron contribution is also negligible leaving the total pressure determined completely by the slope of the symmetry energy. Both the P_0 and P_{asy} increase with density with rates determined separately by the respective density dependences of the SNM EOS and the symmetry energy. In the region around $\rho_0 \sim 2.5\rho_0$, the P_{asy} dominates over the P_0 using most EOSs available. At higher densities, the SNM pressure P_0 dominates while the P_{asy} also plays an important role depending on the high-density behaviors of nuclear symmetry energy (Li & Steiner 2006). The exact transition of dominance from P_{asy} to P_0 depends on the stiffnesses of both the SNM EOS and the symmetry energy. It is also well known that the radius $R_{1.4}$ of canonical NSs is essentially determined by the pressure at densities around $\rho_0 \sim 2.5\rho_0$ (Lattimer & Prakash 2000) while the maximum mass of NSs is determined by the pressure at higher densities reached in the core. Thus, the knowledge about the density dependence of nuclear symmetry energy is important for understanding measurements of both the masses and especially the radii of NSs. Moreover, the critical densities for forming hyperons (Sumiyoshi & Toki 1994; Lee 1996; Kubis & Kutschera 2003; Providência et al. 2019), $\Delta(1232)$ resonances (Drago et al. 2014; Cai et al. 2015; Zhu et al. 2016; Sahoo et al. 2018; Ribes et al. 2019), kaon condensation (Odrzywolek & Kutschera 2009) and the quark phase (Ditoro et al. 2010; Wu & Shen 2019) are also known to depend sensitively on the high-density nuclear symmetry energy. Information about the latter is thus a prerequisite for exploring the evolution of NS matter phase diagram in the isospin dimension. Once the $E_{\text{sym}}(\rho)$ is better determined and hopefully with more astrophysical data, it would be interesting to introduce extra model parameters characterizing the physics associated with the exotic particles and/or new phases predicted to appear in super-dense neutron-rich matter. With the very limited data available and expensive computational costs of simultaneously inferring a lot more than the six EOS parameters we already have in the minimum NS model consisting of only nucleons and two leptons, our goals in this work are conservative and practical. However, inferring new physics parameters associated with the exotic degrees of freedom and new phases in super-dense neutron-rich matter from astrophysical data by extending the model used in the present work are high on our working agenda.

To constrain the EOS of ultra-dense neutron-rich nuclear matter has been a longstanding goal of several branches of astrophysics and astronomy. It is a major science driver in building several new research facilities, such as var-

ious advanced X-ray observatories and earth-based large telescopes as well as gravitational wave detectors on earth and in space. In particular, ongoing and planned observations (Watts et al. 2016; Özel & Freire 2016; Watts 2019; Bogdanov et al. 2019; Fonseca et al. 2019) with, e.g., Chandra, XMM-Newton, Neutron Star Interior Composition Explorer [NICER), the upgraded LIGO and VIRGO gravitational wave detector, are all aiming at measuring more precisely the mass-radius correlations of NSs to help constrain the EOS of dense neutron-rich nuclear matter. In the near future, Athena: Advanced Telescope for High-ENergy Astrophysics (Athena 2014), eXTP: enhanced X-ray Timing and Polarimetry (Zhang et al. 2019), Large Observatory for x-ray Timing (LOFT-P) (Wilson-Hodge et al. 2016) and STROBE-X: Spectroscopic Time-Resolving Observatory for Broadband Energy X-rays (Ray et al. 2019) will further improve precisions of the mass and/or radius measurements. On the other hand, terrestrial nuclear reactions induced by high-energy radioactive ion beams at several new facilities under construction in several countries are also expected to provide improved constraints on the EOS, especially its symmetry energy term, of dense neutron-rich nuclear matter, see, e.g., refs. (Balantekin et al. 2014; Hong et al. 2014; Tamii et al. 2014; Li 2017; Trautmann 2019).

Table 1. The radius $R_{1.4}$ data used in this work.

Radius $R_{1.4}$ (km) (90% confidence level)	Source	Reference
$11.9^{+1.4}_{-1.4}$	GW170817	(Abbott et al. 2018)
$10.8^{+2.1}_{-1.6}$	GW170817	(De et al. 2018)
$11.7^{+1.1}_{-1.1}$	QLMXBs	(Lattimer & Steiner 2014)
$11.9 \pm 0.8, 10.8 \pm 0.8, 11.7 \pm 0.8$	Imagined case-1	this work
11.9 ± 0.8	Imagined case-2	this work

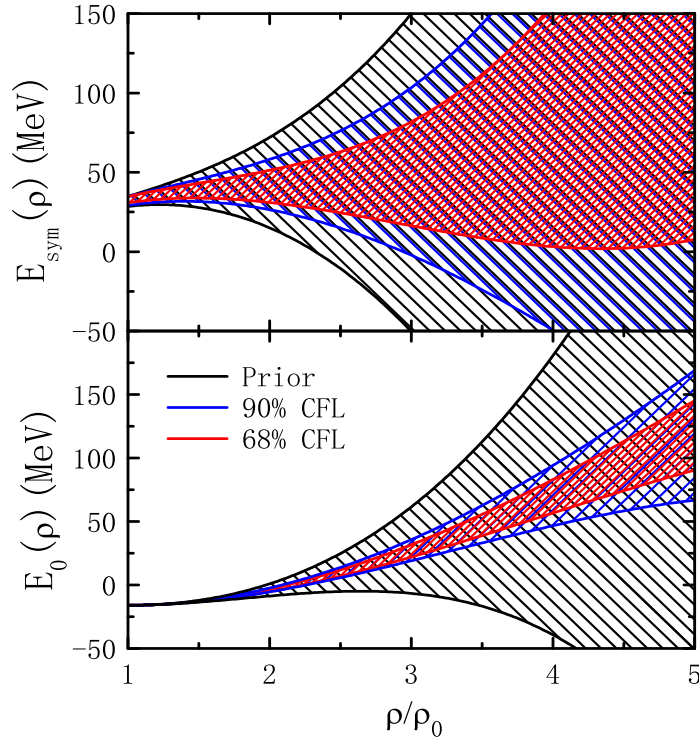


Figure 1. Nuclear symmetry energy (upper) and the energy per nucleon in symmetric nuclear matter (lower) as functions of the reduced density ρ/ρ_0 . The black, blue and red shadows represent the prior as well as the 90% and 68% credible areas of the posterior functions inferred from the Bayesian analysis in this work using the three radius data listed in Table 1 and all known astrophysical constraints about the EOS of neutron star matter, respectively.

While waiting eagerly with much interest for results from the new observations and experiments, here we report results of a Bayesian inference of high-density nuclear symmetry energy using the latest $R_{1.4}$ radius data for canonical

NSs extracted from analyzing the GW170817 and quiescent low-mass X-ray binaries (QLMXBs) as listed in Table 1 under the condition that any EOS has to be stiff enough to support the observed maximum NS mass, causal and thermodynamically stable at all densities. While there are still some interesting issues and model dependences in extracting the $R_{1.4}$ from the raw data of both gravitational waves and X-rays, within the quoted errors bars in Table 1 the results from different analyses using various models are largely consistent as discussed in detail in Section 5 of ref. (Li et al. 2019). It is worth emphasizing that while the two NSs involved in GW170817 have significantly different mass ranges, the two independent analyses in refs (Abbott et al. 2018; De et al. 2018) using different approaches all found consistently that the two NSs have essentially identical radii within the specified uncertainties in Table 1. In particular, without any prior restriction on the radii, Abbott et al. (2018) found that the two NSs have the same radius independent of their masses although the radius has different values in different models they used. While in the analyses by De et al. (2018), the two NSs are assumed to have the same radius and they found that the radius is basically independent of the prior mass distributions they assumed for the two NSs. In this study, we took the radii they extracted as for the $R_{1.4}$ consistent with their finding that the radius is mass independent. However, we notice that the error bars of the inferred radii are still large. The possible small mass dependences of the radii predicted by some model EOSs are probably buried in the current uncertainty ranges of the radii.

For comparisons and see how reduced error bars of $R_{1.4}$ data may help us reduce uncertainties of the inferred EOS parameters, we will also use the two imaged cases listed at the bottom of Table 1. The three real data points have 6-13% 1σ statistical errors and their mean values vary by about 1 km from each other, representing approximately a 10% systematic error of the real case. The imaginary case-1 has the same $R_{1.4}$ mean values as the real data set but a constant absolute error of 0.8 km at 90% confidence level (CFL). It represents a case of about 4-5% statistical error of each data point at 68% CFL but the same systematic error as the real case. While the imaginary case-2 represents a situation where all measurements give the same result as the first data point of imaginary case-1, i.e., no systematic error but a 4% 1σ statistical error around the mean value of $R_{1.4} = 11.9$ km. Comparisons of results from these 3 cases serve well our main purposes in this work. We would like to establish a generally useful reference for measuring the progress in determining the high-density nuclear symmetry to be brought to us hopefully soon by the new astrophysical observations and terrestrial experiments. Besides being useful for screening predictions of nuclear many-body theories, the obtained posterior probability distribution functions (PDFs) of six parameters involved in an explicitly isospin-dependent parametric EOS are used to construct the confidence boundaries of both the SNM EOS $E_0(\rho)$ and symmetry energy $E_{\text{sym}}(\rho)$.

For busy readers who are eager to know quickly the most important conclusions of our work, shown in Figure 1¹ is the inferred symmetry energy $E_{\text{sym}}(\rho)$ and the SNM EOS $E_0(\rho)$ as functions of the reduced density ρ/ρ_0 using the real data set. The black, blue and red shadows represent the prior, 90% and 68% credible areas, respectively. Compared to what we currently know (the prior functions) mostly based on nuclear experiments and theories, the refinement brought in by the astrophysical observations is very significant. More specifically, at densities between $\rho_0 - 2.5\rho_0$, both the $E_0(\rho)$ and $E_{\text{sym}}(\rho)$ are constrained reasonably tightly within their respective narrow bands approximately independent of whether we parameterize the $E_0(\rho)$ with 2 or 3 terms and the $E_{\text{sym}}(\rho)$ with 3 or 4 terms, respectively. In particular, the symmetry energy at $2\rho_0$ is determined to be $E_{\text{sym}}(2\rho_0) = 39.2^{+12.1}_{-8.2}$ MeV at 68% CFL. However, at densities above about $2.5\rho_0$, the 68% confidence boundaries for both the $E_0(\rho)$ and $E_{\text{sym}}(\rho)$ diverge depending strongly on the EOS parameterizations used.

The rest of the paper is organized as follows: in the next section we outline the explicitly isospin-dependent parametric EOS for modeling NSs containing neutrons, protons, electrons and muons (the $npe\mu$ matter). We then outline the steps we used within the Markov-Chain Monte Carlo (MCMC) approach to sample the posterior PDFs of six EOS parameters. In section 3, we present and discuss the posterior PDFs and correlations of the EOS parameters under various conditions to explore possible model dependences as well as effects of uncertain factors and data accuracies. We then construct the 68% confidence boundaries of both the SNM EOS $E_0(\rho)$ and symmetry energy $E_{\text{sym}}(\rho)$. Finally, we summarize our main findings.

2. THEORETICAL FRAMEWORK

¹ The $E_0(\rho)$ and $E_{\text{sym}}(\rho)$ shown here should be used jointly in Eq. 1 with the δ determined self-consistently by the β equilibrium and charge neutrality conditions. As we shall discuss, when the $E_{\text{sym}}(\rho)$ is zero or negative, the system becomes pure neutron matter. The negative value along the lower boundary of $E_0(\rho)$ at high densities does not necessarily mean that SNM at these densities are stable and energetically more preferred.

Table 2. Prior ranges of the six EOS parameters used

Parameters	Lower limit	Upper limit (MeV)
K_0	220	260
J_0	-800	400
K_{sym}	-400	100
J_{sym}	-200	800
L	30	90
$E_{\text{sym}}(\rho_0)$	28.5	34.9

2.1. Explicitly isospin-dependent parametric EOS for the cores of neutron stars

In Bayesian inferences of nuclear EOSs from astrophysical data, various parametric and non-parametric representations of the EOS at supra-saturation densities have been used in the literature, see, e.g. refs. (Steiner et al. 2010; Alvarez-Castillo et al. 2016; Özel et al. 2016; Raithel et al. 2017; Riley et al. 2018; Raaijmakers et al. 2018; Lim & Holt 2019; Miller et al. 2019; Landry & Essick 2019; Greif et al. 2019). While there is relatively little disagreement about the EOSs of the low-density crust and nuclear matter near ρ_0 . For a very recent review of different ways of parameterizing the EOSs, their advantages, drawbacks, technical applicabilities and proposals of reducing the prior-dependence in Bayesian inference of EOS parameters, we refer the reader to Section 2.4 of ref. (Baiotti 2019) and references therein. Because the pressure in NSs at β equilibrium is a function only of the density, namely the pressure $P(\rho)$ is barotropic, most studies parameterize the pressure directly as a function of density using piecewise-polytropic parameterizations (Lindblom 2010), the spectral parameterizations (Lindblom 2018) or parameterizations generated with a Gaussian process (Landry & Essick 2019). Indeed, the EOS given in terms of $P(\rho)$ is enough for solving the Tolman-Oppenheimer-Volkov (TOV) equations (Tolman 1934; Oppenheimer & Volkoff 1939) to obtain a mass-radius sequence. However, to obtain accurate information about the high-density nuclear symmetry energy and the corresponding density profile of proton fraction $x_p(\rho)$ in the cores of NSs at β equilibrium, one has to construct the pressure $P(\rho)$ by parameterizing directly the underlying $E_0(\rho)$ and $E_{\text{sym}}(\rho)$, separately. Since the $x_p(\rho)$ in NSs at β equilibrium is uniquely determined by the $E_{\text{sym}}(\rho)$ through the chemical equilibrium and charge neutrality conditions, the pressure $P(\rho)$ can be easily constructed from the parameterized $E_0(\rho)$ and $E_{\text{sym}}(\rho)$. Such procedure has been used in a number of studies for several purposes in the literature, see, e.g., refs. (Oyamatsu & Iida 2007; Sotani et al. 2012; Margueron et al. 2017a,b; Zhang et al. 2018; Malik et al. 2018; Lim & Holt 2019; Li & Sedrakian 2019), albeit sometimes using different numbers of parameters for either one or both of the $E_0(\rho)$ and $E_{\text{sym}}(\rho)$. For a recent review, see, ref. (Li et al. 2019). In this work, we use this procedure in preparing the NS EOS for our Bayesian inference of the high-density nuclear symmetry energy. Details of constructing this NS EOS model were given in refs. (Zhang et al. 2018; Zhang & Li 2019a,b,c). In the previous work, however, we fixed the low-order EOS parameters at their currently known most probable values, then several NS observables were inverted in the three-dimensional high-density EOS parameter space. In the Bayesian analyses here, we infer the PDFs of all six EOS parameters from the $R_{1.4}$ data discussed in the previous section. Thus, in the remainder of this section, we only summarize the parts of our EOS parameterization most relevant for the Bayesian analyses.

Within the minimal model of NSs consisting of neutrons, protons, electrons and muons at β equilibrium, the pressure

$$P(\rho, \delta) = \rho^2 \frac{d\epsilon(\rho, \delta)/\rho}{d\rho} \quad (3)$$

is determined by the energy density

$$\epsilon(\rho, \delta) = \rho[E(\rho, \delta) + M_N] + \epsilon_l(\rho, \delta), \quad (4)$$

where M_N represents the average nucleon mass and $\epsilon_l(\rho, \delta)$ denotes the lepton energy density. As shown by Eq. (1), the nucleon energy $E(\rho, \delta)$ is given by the SNM EOS $E_0(\rho)$ and the symmetry energy $E_{\text{sym}}(\rho)$ which are parameterized respectively according to

$$E_0(\rho) = E_0(\rho_0) + \frac{K_0}{2} \left(\frac{\rho - \rho_0}{3\rho_0} \right)^2 + \frac{J_0}{6} \left(\frac{\rho - \rho_0}{3\rho_0} \right)^3, \quad (5)$$

where $E_0(\rho_0) = -15.9$ MeV at $\rho_0 = 0.16$ nucleons/fm³ (both the $E_0(\rho_0)$ and ρ_0 are fixed at these values in this work) and

$$E_{\text{sym}}(\rho) = E_{\text{sym}}(\rho_0) + L\left(\frac{\rho - \rho_0}{3\rho_0}\right) + \frac{K_{\text{sym}}}{2}\left(\frac{\rho - \rho_0}{3\rho_0}\right)^2 + \frac{J_{\text{sym}}}{6}\left(\frac{\rho - \rho_0}{3\rho_0}\right)^3. \quad (6)$$

As discussed earlier (Zhang et al. 2018; Zhang & Li 2019a), the above parameterizations naturally become the Taylor expansions in the limit of $\rho \rightarrow \rho_0$. Compared to the widely used multi-segment polytropic EOSs often with connecting densities/pressures of different density regions as parameters, the asymptotic boundary conditions of the above parameterizations near ρ_0 and $\delta = 0$ facilitate the use of prior knowledge on the EOS provided by terrestrial nuclear laboratory experiments and/or nuclear theories. Near ρ_0 when the above parameterizations become Taylor expansions of the nuclear energy density functionals, the EOS parameters start obtaining their asymptotic physical meanings. Namely, the K_0 parameter becomes the incompressibility of SNM $K_0 = 9\rho_0^2[\partial^2 E_0(\rho)/\partial \rho^2]|_{\rho=\rho_0}$ and the J_0 parameter becomes the skewness of SNM $J_0 = 27\rho_0^3[\partial^3 E_0(\rho)/\partial \rho^3]|_{\rho=\rho_0}$ at saturation density, while the four parameters involved in the $E_{\text{sym}}(\rho)$ become the magnitude $E_{\text{sym}}(\rho_0)$, slope $L = 3\rho_0[\partial E_{\text{sym}}(\rho)/\partial \rho]|_{\rho=\rho_0}$, curvature $K_{\text{sym}} = 9\rho_0^2[\partial^2 E_{\text{sym}}(\rho)/\partial \rho^2]|_{\rho=\rho_0}$ and skewness $J_{\text{sym}} = 27\rho_0^3[\partial^3 E_{\text{sym}}(\rho)/\partial \rho^3]|_{\rho=\rho_0}$ of nuclear symmetry energy at saturation density, respectively. These connections between the EOS parameters and the characteristics of nuclear matter and symmetry energy at ρ_0 provide us naturally some useful information about the EOS parameters. Summarized in Table 2 are the currently known ranges of the asymptotic values of the EOS parameters near ρ_0 based on systematics of terrestrial nuclear experiments and predictions of various nuclear theories. As indicated in Table 2, while the K_0 , $E_{\text{sym}}(\rho_0)$ and L have been constrained to relatively small ranges (Danielewicz et al. 2002; Li & Han 2013; Oertel et al. 2017; Shlomo et al. 2006; Piekarewicz 2010), the J_0 , K_{sym} and J_{sym} describing the EOS of dense neutron-rich matter are only poorly known in a wide range (Tews et al. 2017; Zhang et al. 2017). In the Bayesian inferences of their PDFs from astrophysical data, we use these ranges as the prior ranges. We use uniform prior PDFs within these ranges for the six EOS parameters as there is no known physical preference for any specific values of these parameters within the ranges specified. For example, the ranges of $E_{\text{sym}}(\rho_0)$ and L were obtained from the systematics of 53 different analyses of some terrestrial experiments and astrophysical observations (Li & Han 2013; Oertel et al. 2017; Li et al. 2019). At present and to our best knowledge, one can only reasonably assume *a priori* that the EOS parameters can equally take any value within the ranges listed.

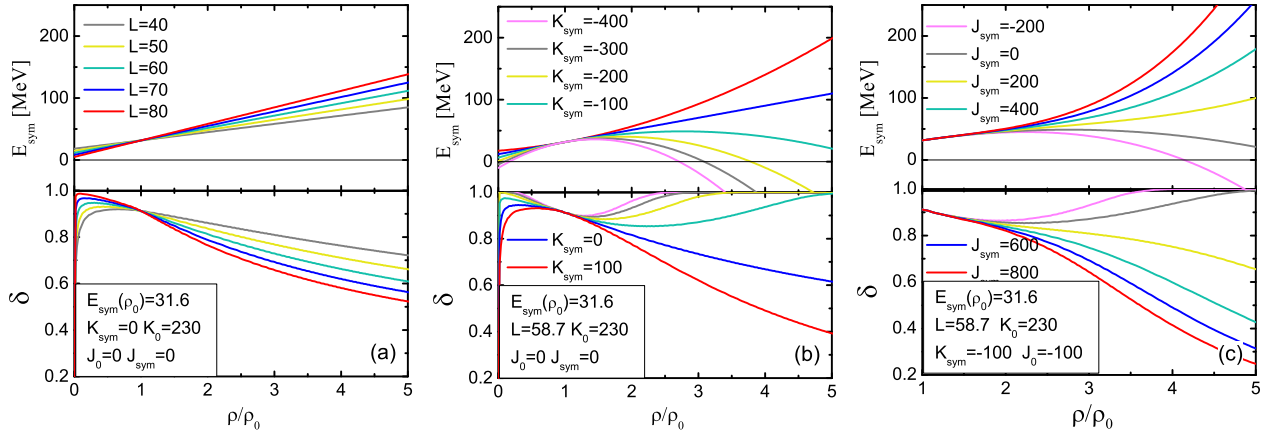


Figure 2. The symmetry energy $E_{\text{sym}}(\rho)$ and isospin asymmetry $\delta(\rho)$ in neutron star matter at β -equilibrium as a function of the reduced density ρ/ρ_0 for $L = 40, 50, 60, 70$, and 80 MeV (a), $K_{\text{sym}} = -400, -300, -200, -100, 0$, and 100 MeV (b), and $J_{\text{sym}} = -200, 0, 200, 400, 600$ and 800 MeV (c), respectively. Taken from ref. (Zhang et al. 2018).

The two parameterizations of Eq. (5) and Eq. (6) are combined using Eq. (1) to obtain the pressure $P(\rho)$ as a function of density only once the density-profile of the isospin asymmetry $\delta(\rho)$ (or the proton fraction $x_p(\rho)$) is calculated self-consistently from the β -equilibrium condition $\mu_n - \mu_p = \mu_e = \mu_\mu \approx 4\delta E_{\text{sym}}(\rho)$ and the charge neutrality condition $\rho_p = \rho_e + \rho_\mu$. The chemical potential for a particle i is obtained from $\mu_i = \partial \epsilon(\rho, \delta)/\partial \rho_i$. As an illustration, shown in Fig. 2 are samples of the $E_{\text{sym}}(\rho)$ and the corresponding $\delta(\rho)$ values generated by varying individually the L , K_{sym} and J_{sym} parameters while all other parameters are fixed as indicated in the figure: (a) $L = 40, 50, 60, 70$, and 80 MeV, (b) $K_{\text{sym}} = -400, -300, -200, -100, 0$, and 100 MeV, and (c) $J_{\text{sym}} = -200, 0, 200, 400, 600$ and 800 MeV. Clearly, very diverse behaviors of the $E_{\text{sym}}(\rho)$ and the corresponding $\delta(\rho)$ can be sampled. As expected, the L , K_{sym}

and J_{sym} affect gradually more significantly the high-density behavior of the symmetry energy. Interestingly, because of the $E_{\text{sym}}(\rho) \cdot \delta^2$ term in the nuclear energy density functional, a higher value of $E_{\text{sym}}(\rho)$ will lead to a smaller $\delta(\rho)$ at β equilibrium. The ramifications of this effect, regarded as the isospin fractionation, is well known in nuclear physics and has been studied extensively in heavy-ion collisions at intermediate energies, see, e.g., refs. (Muller & Serot 1995; Xu et al. 2000; Li et al. 2008).

Theoretically, the parameterization of $E_{\text{sym}}(\rho)$ may not always approach zero at zero density when all of its parameters are randomly generated. While one can cure this completely by introducing additional parameters or use different forms at very low densities, see, e.g., refs. (Margueron et al. 2017a; Holt et al. 2018), practically we avoided this problem by adopting the NV EOS (Negele & Vautherin 1973) for the inner crust and the BPS EOS (Baym et al. 1971b) for the outer crust, respectively. The crust-core transition density and pressure are determined by investigating the thermodynamical instability of the uniform matter in the core (Zhang et al. 2018). When the incompressibility of $n\rho\mu$ matter (Kubis 2004, 2007; Lattimer & Prakash 2007)

$$K_\mu = \rho^2 \frac{d^2 E_0}{d\rho^2} + 2\rho \frac{dE_0}{d\rho} + \delta^2 \left[\rho^2 \frac{d^2 E_{\text{sym}}}{d\rho^2} + 2\rho \frac{dE_{\text{sym}}}{d\rho} - 2E_{\text{sym}}^{-1} (\rho \frac{dE_{\text{sym}}}{d\rho})^2 \right] \quad (7)$$

becomes negative at low densities, the uniform matter becomes unstable against the formation of clusters. Numerical examples of the crust-core transition density and pressure can be found in ref. (Zhang et al. 2018). Clearly, the K_μ depends mainly on the K_0 , L and K_{sym} . For fast MCMC samplings, we have prepared a table of the crust-core transition density and pressure as functions of K_0 , L and K_{sym} with a bin size of 5 MeV. The latter defines the internal energy resolution of our Bayesian inference. This table is available up on request from the authors of this work.

2.2. Bayesian Inference Approach

As discussed above and also in refs. (Zhang et al. 2018; Zhang & Li 2019a), the Eqs. (5) and (6) have the dual meanings (either as parameterizations or Taylor expansions) near the saturation density, but when applied to high densities, they are simply parameterizations. In refs. (Zhang et al. 2018; Zhang & Li 2019a), by fixing the three low-order parameters K_0 , $E_{\text{sym}}(\rho_0)$ and L at their most probable values currently known, effects of only the three high-density (order) parameters J_0 , K_{sym} and J_{sym} were studied by inverting individually several observables directly in the three-dimensional high-density EOS parameter space. While the results are very useful, not only effects of uncertainties of the low-order parameters but also correlations among the EOS parameters were not considered or treated on equal footing. In the present work, we treat the six parameters in Eqs. (5) and (6) all as free parameters to be constrained simultaneously by the same astrophysical data and several known constraints using the Bayesian inference approach.

The key in this approach is the calculation of the posterior PDFs of the model EOS parameters through the MCMC sampling. For completeness, we recall here the Bayes' theorem

$$P(\mathcal{M}|D) = \frac{P(D|\mathcal{M})P(\mathcal{M})}{\int P(D|\mathcal{M})P(\mathcal{M})d\mathcal{M}}, \quad (8)$$

where $P(\mathcal{M}|D)$ is the posterior probability for the model \mathcal{M} given the data set D , which is what we are seeking here, while $P(D|\mathcal{M})$ is the likelihood function or the conditional probability for a given theoretical model \mathcal{M} to predict correctly the data D , and $P(\mathcal{M})$ denotes the prior probability of the model \mathcal{M} before being confronted with the data. The denominator in Eq. (8) is the normalization constant. We sample uniformly each EOS parameter p_i randomly between its minimum $p_{\text{min},i}$ and maximum $p_{\text{max},i}$ values given in Table 2 according to $p_i = p_{\text{min},i} + (p_{\text{max},i} - p_{\text{min},i})x$ with the random number x between 0 and 1. Using the generated EOS parameters, $p_{i=1,2,\dots,6}$, one can construct the NS EOS model $\mathcal{M}(p_{1,2,\dots,6})$ as we outlined in the previous subsection. The NS mass-radius sequence is then obtained by solving the TOV equations. The resulting theoretical radius $R_{\text{th},j}$ is subsequently used to calculate the likelihood of this EOS parameter set with respect to the observed radius $R_{\text{obs},j}$ with $j = 1, 2, 3$ in the data set $D(R_{1,2,3})$ given in Table 1 according to

$$P[D(R_{1,2,3})|\mathcal{M}(p_{1,2,\dots,6})] = \prod_{j=1}^3 \frac{1}{\sqrt{2\pi}\sigma_{\text{obs},j}} \exp\left[-\frac{(R_{\text{th},j} - R_{\text{obs},j})^2}{2\sigma_{\text{obs},j}^2}\right], \quad (9)$$

where $\sigma_{\text{obs},j}$ is the 1σ error bar of the observation j . For the radius data given in Table 1, the upper/lower error bar in radius at 90% CFL is 1.645σ . For the asymmetric case with different upper and lower error bars, we took their average before calculating the σ value. In applying the approach to canonical NSs with the same mass of $1.4 M_\odot$, $R_{\text{th},j} \equiv R_{1.4}^{\text{th}}$ is independent of the index j , i.e., we treat the three radii in the data set as from independent observations of the

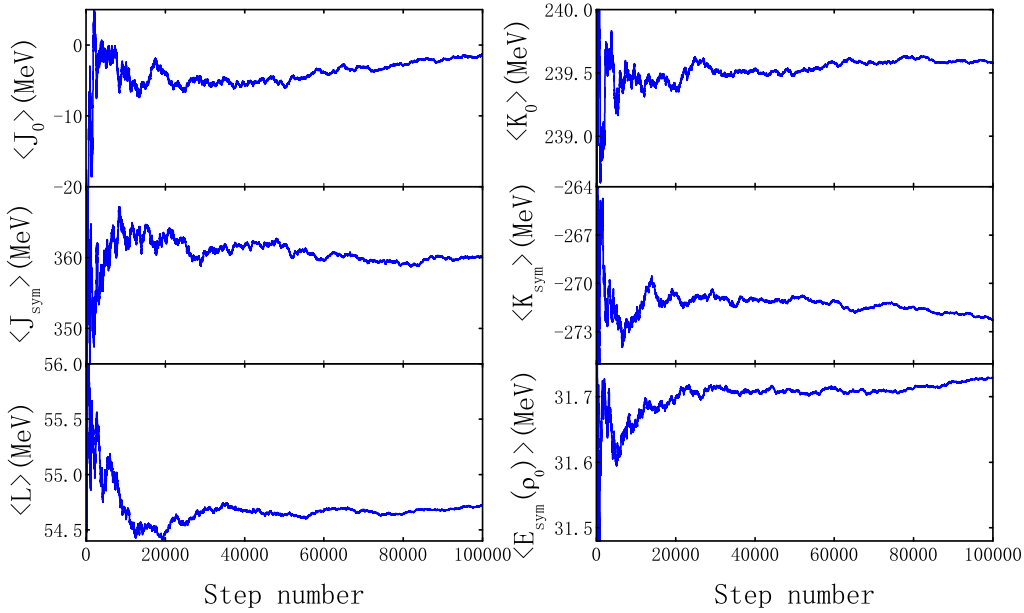


Figure 3. Mean values of the six EOS parameters as functions of the step number.

same NS. We will calculate both the marginalized PDFs of all individual EOS parameters and the two-parameter correlations by integrating over all other parameters. In particular, the PDF of a model parameter p_i is analytically given by

$$P(p_i|D) = \frac{\int P(D|\mathcal{M}) dp_1 dp_2 \cdots dp_{i-1} dp_{i+1} \cdots dp_6}{\int P(D|\mathcal{M}) P(\mathcal{M}) dp_1 dp_2 \cdots dp_6}, \quad (10)$$

while the correlation function between any two parameters p_i and p_j can be similarly written as an integral of the $P(D|\mathcal{M})$ over all parameters except the p_i and p_j themselves. Numerically, the $P[D(R_{1,2,3})|\mathcal{M}(p_{1,2,\dots,6})]$ is simulated using the MCMC sampling approach. The integrations are also done naturally using the Monte Carlo approach. Namely, the PDF of a model parameter p_i is obtained by summing up the accepted $P(D|\mathcal{M})$ at all steps in the MCMC process and the sum is binned only according to the value of p_i regardless of all other parameters. While the two-dimensional correlation function between the two parameters p_i and p_j is obtained by binning the sum according to both the p_i and p_j regardless of the values of all other parameters. While it is necessary to normalize the PDFs of single EOS parameters individually, unnormalized correlation functions are sufficient for all practical purposes.

Many MCMC techniques are available in the literature, in this work we adopted the Metropolis-Hastings algorithm (Metropolis et al. 1953; Hastings 1970). In developing our MCMC package in Fortran 90, we used as an example the MCMC code developed in ref. (Keating & Cherry 2009) following the procedure given in ref. (Zhang et al. 2006). It is well known that because the MCMC process does not start from an equilibrium distribution, initial samples in the so-called burn-in period have to be thrown away (Trotta 2017). The adequate burn-in step numbers are those after which either the posterior densities or means of the model parameters remain approximately constants on their trace plots during the MCMC sampling. Shown in Figure 3 are the mean values for our six EOS parameters as functions of the step number. It is seen that after about 40,000 steps, the mean values for all of the parameters stay approximately constants. Thus, we take 40,000 burn-in steps in all calculations performed in this work.

3. RESULTS AND DISCUSSIONS

All EOSs we constructed satisfy the following default conditions: (i) The crust-core transition pressure stays positive; (ii) The thermodynamical stability condition, $dP/d\varepsilon \geq 0$, is satisfied at all densities; (iii) The causality condition is enforced at all densities; (iv) The generated NS EOS should be stiff enough to support the currently observed maximum mass of NSs. We consider the maximum mass as a variable and discuss its effects on what we infer about the EOS parameters by using either a sharp cut-off at 1.97, 2.01 or 2.17 M_\odot or a Gaussian distribution for the maximum mass

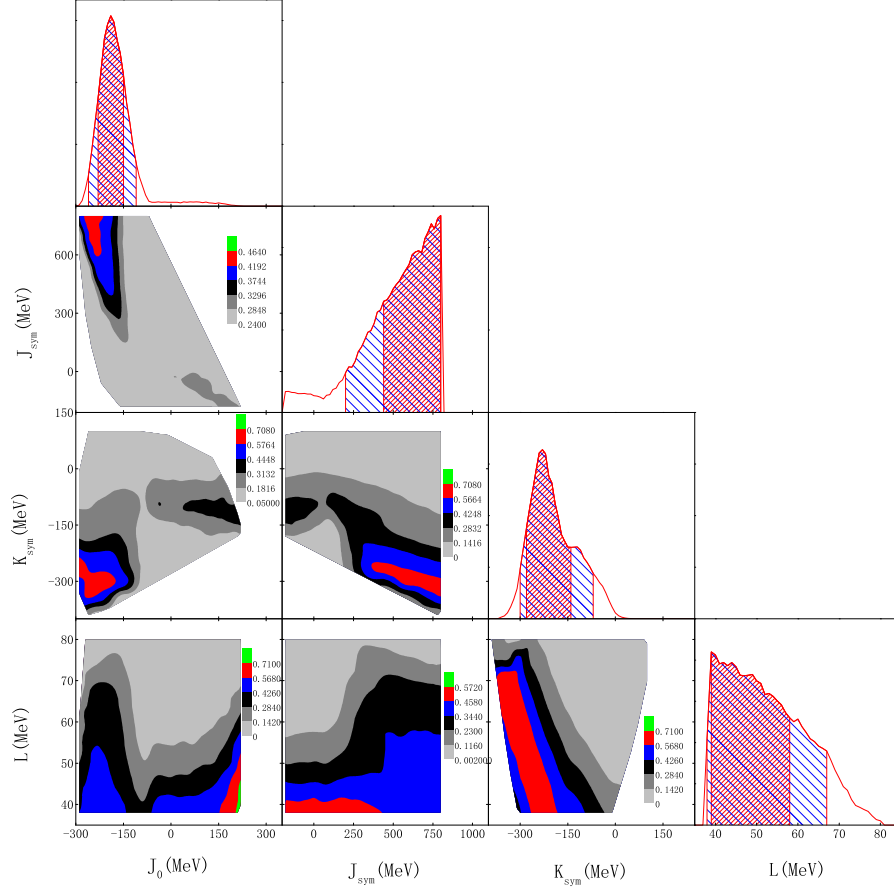


Figure 4. Posterior probability distribution functions and correlations of high-density EOS parameters.

Table 3. Most probable values of the EOS parameters and their 68%, 90% confidence boundaries

Parameter (MeV)	68% boundaries	90% boundaries
J_0	-190^{+40}_{-40}	-190^{+80}_{-70}
K_0	222^{+26}_{-0}	222^{+0}_{-35}
J_{sym}	800^{+0}_{-360}	800^{+0}_{-600}
K_{sym}	-230^{+90}_{-50}	-230^{+160}_{-70}
L	39^{+19}_{-0}	39^{+28}_{-1}
$E_{\text{sym}}(\rho_0)$	$34^{+0.8}_{-4.8}$	$34^{+0.8}_{-3.2}$

centered around 2.01 or 2.17 M_\odot with a 1σ error of 0.04 or 0.11 M_\odot , respectively. In presenting and discussing our results in the following, we use as a baseline the default result obtained by using the sharp cut-off at 1.97 M_\odot , namely all EOSs have to be able to support NSs at least as massive as 1.97 M_\odot , and the three real $R_{1.4}$ radius data given in Table 1. Based on all the information we have so far, conclusions based on the default results are the most realistic and conservative. Results from variations of the physics conditions and/or using the imagined data sets will then be compared with the default results. We focus on the marginalized PDFs of the model parameters and their correlations induced by the physics conditions and/or the radius data. The $E_0(\rho)$ and $E_{\text{sym}}(\rho)$ at various confidence levels in relevant cases will be constructed. Since the PDFs of EOS parameters are asymmetric in most cases, in presenting our results we use the highest posterior density interval (Turkkan 2014) to locate the 68% (90%) credible intervals

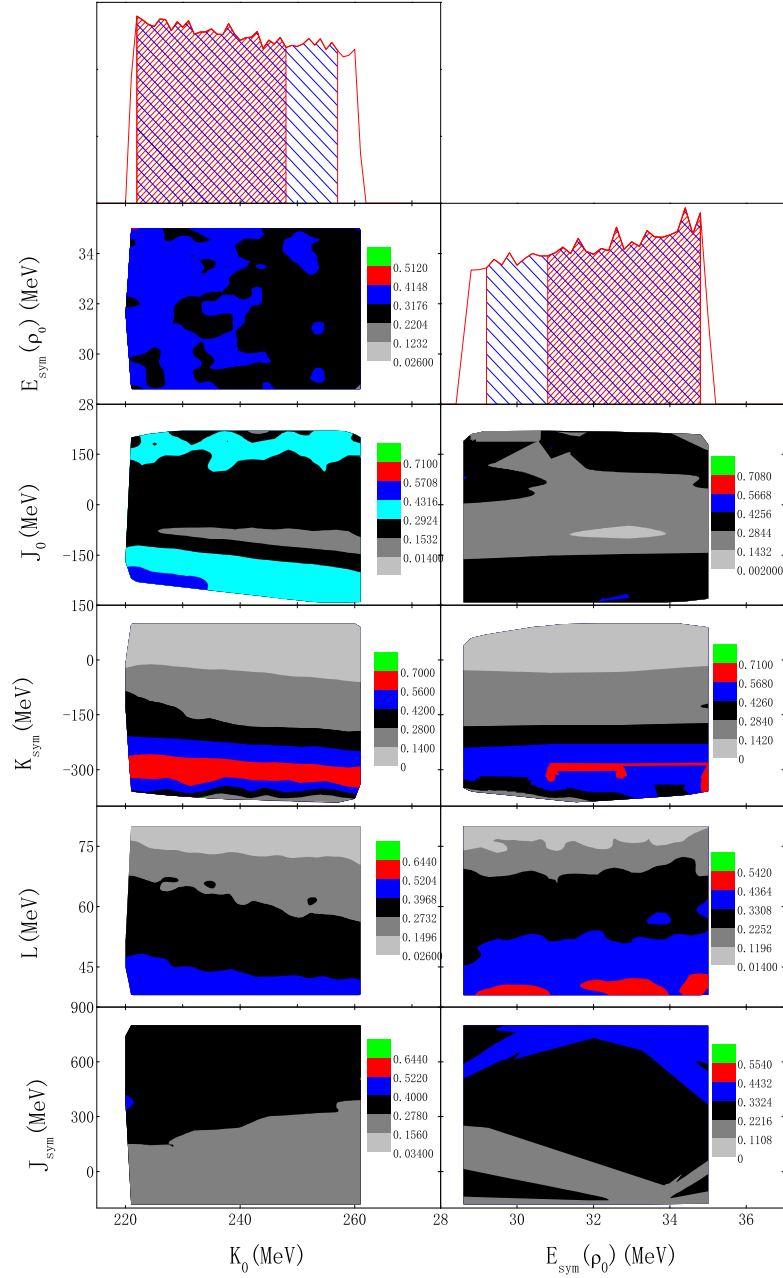


Figure 5. Posterior probability distribution functions of low-density EOS parameters and their correlations with the high-density EOS parameters.

according to

$$\int_{p_{iL}}^{p_{iU}} \text{PDF}(p_i) dp_i = 0.68 \text{ (0.90)}, \quad (11)$$

where (p_{iL}, p_{iU}) is the (lower, upper) limit of the corresponding narrowest interval of the parameter p_i surrounding the maximum value of the $\text{PDF}(p_i)$.

3.1. The posterior PDFs and correlations of EOS parameters

Shown in Figures 4 and 5 are the marginalized posterior PDFs of the six EOS parameters and their correlations. The blue and red shadows outline the 90% and 68% credible intervals of the PDFs, respectively. The most probable values of the six EOS parameters and their 68%, 90% confidence boundaries are summarized in Table 3. Several interesting observations can be made:

- The J_0 and K_{sym} parameters are relatively well constrained, and larger values of J_{sym} but smaller values of L are preferred while the saturation parameters K_0 and $E_{\text{sym}}(\rho_0)$, as shown in Figure 5, are essentially not affected by the radius data and the default physics conditions used in this baseline calculation compared to their prior ranges given in Table 2. These features are easily understandable. Since the average density in canonical NSs with $1.4 M_\odot$ is not so high, it is difficult to constrain the high-density symmetry energy parameter J_{sym} by using the $R_{1.4}$ data. As discussed in refs. (Lattimer & Prakash 2000, 2001), the radius of canonical NSs is most sensitive to the pressure around $2\rho_0$. One thus expects that the $R_{1.4}$ data is most useful for constraining EOS parameters having largest influences on the pressure around $2\rho_0$. This appears to be case for the K_{sym} parameter. It plays a pivotal role in determining the pressure at intermediate densities reached in canonical NSs, and thus being narrowed down to a small range by the $R_{1.4}$ data used in this analysis. The parameter J_0 characterizing the high-density behavior of the SNM EOS $E_0(\rho)$ is sensitive to the NS maximum mass but not to the radius of canonical NSs (Zhang et al. 2018; Zhang & Li 2019a). It is the condition that all EOSs should be stiff enough to support NSs at least as massive as $1.97 M_\odot$ that narrowed down the J_0 parameter range. We shall discuss in more detail the individual roles of J_0 and J_{sym} in subsections 4.2 and 4.3, separately, as they are not always considered simultaneously in Bayesian inferences of the nuclear EOS in the literature.
- Generally speaking, mathematically one expects that a given parameter is most likely to correlate with its nearest neighbors used in parameterizing a specific function, e.g., K_{sym} with its left neighbor L and right neighbor J_{sym} in parameterizing the $E_{\text{sym}}(\rho)$. All of the six EOS parameters started as independent ones, they become correlated basically by satisfying several energy conservation as well as chemical and mechanical equilibrium conditions when the radii and masses from solving the TOV equations are required to reproduce the radius data within certain ranges under the conditions specified. Two near-by parameters in a given function can easily compensate each other to reproduce the same data under the same condition. It is thus not surprising that there are stronger anti-correlations between L and K_{sym} as well as between J_{sym} and K_{sym} , but only very weak correlations between the saturation-density parameters and the high-density parameters.

Two parameters used in parameterizing the $E_0(\rho)$ and $E_{\text{sym}}(\rho)$ may also be correlated through the total nucleon specific energy $E(\rho, \delta)$ in Eq. (1). Depending on the resulting value of δ , two parameters from the two parameterizations generally have to be at the same order in density to have strong correlations. For example, the J_0 and J_{sym} both at the third-order in density are expected to be strongly correlated when the δ is close to 1 achieved when the symmetry energy is super-soft especially with negative J_{sym} as shown in Fig. 2. However, correlations between low-order (e.g., K_0) and high-order (e.g., J_{sym}) parameters are expected to be very weak. In fact, a strong anti-correlation between J_0 and J_{sym} is necessary in order to support the same observed NS maximum mass. Namely, an increasing J_0 is needed when J_{sym} is decreasing to keep the high-density pressure strong enough to support the same massive NSs. In addition, an anti-correlation between L and K_{sym} exists independent of what values the J_{sym} takes to keep the same radius $R_{1.4}$. These features are consistent with those found from studying the constant surfaces of radii, speed of sound and/or the maximum mass in the EOS parameter spaces (Zhang & Li 2019a,b). It is also interesting to note that there is a positive correlation between J_0 and K_{sym} . This is understandable from the anti-correlation between J_0 and J_{sym} , and the anti-correlation between J_{sym} and K_{sym} . However, this finding is different from that found in ref. (Baillot et al. 2019) where a strong anti-correlation between J_0 and K_{sym} was observed while a similarly strong anti-correlation between L and K_{sym} was also found as in our present work. We found that this is due to the fact that the J_{sym} was set to zero in ref. (Baillot et al. 2019). In fact, results very similar to theirs are obtained when we set $J_{\text{sym}}=0$ in the present work, as shown in Figure 6 and to be discussed in more detail in the subsection 4.3. It is seen that now an anti-correlation between the J_0 and K_{sym} appears while that between the L and K_{sym} stays the same.

- Some of the PDFs have extended tails and/or shoulders due to the correlations among the six EOS parameters. For example, the PDF of J_0 has an appreciable tail extending to large positive J_0 values. Much efforts have been devoted to predicting the value of J_0 over the past years. For example, in ref. (Farine et al. 1997), $J_0 = -700 \pm 500$

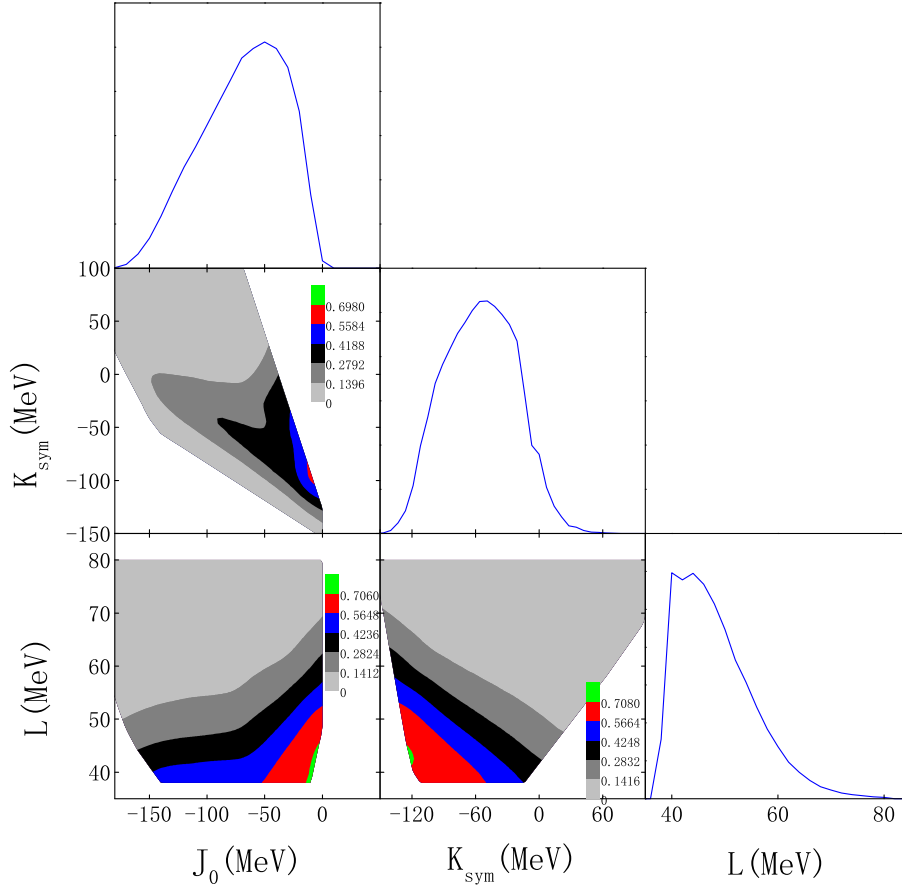


Figure 6. Posterior probability distribution functions and correlations of high-density EOS parameters by setting $J_{\text{sym}} = 0$.

MeV was obtained by analyzing nuclear giant monopole resonances. From an earlier Bayesian analysis of some NS data, $J_0 = -280^{+72}_{-410}$ MeV was inferred by assuming $r_{\text{ph}} \gg R$, where r_{ph} and R represent the photospheric and stellar radii, respectively, but $J_0 = -500^{+170}_{-290}$ MeV was obtained with $r_{\text{ph}} = R$ (Steiner et al. 2010). By using a correlation analysis method based on the Skyrme Hartree-Fock energy density functional (Chen 2011), a value of $J_0 = -355 \pm 95$ MeV was estimated. While within a nonlinear relativistic mean field model (Cai & Chen 2014), by combining the constraints imposed by the flow data in heavy-ion collisions (Danielewicz et al. 2002) and the mass of PSR J0348+0432 (Antoniadis et al. 2013), a range of $-494 \text{ MeV} \leq J_0 \leq -10 \text{ MeV}$ for J_0 was inferred.

However, contrast to the mostly negative values of J_0 mentioned above, positive J_0 values with very lower probabilities are allowed as indicated in the top left panel of Figure 4. This is due to the correlations among J_0 , J_{sym} and K_{sym} , especially the correlation between J_0 and J_{sym} . As discussed in ref. (Zhang et al. 2018) and illustrated in Figure 2, extremely small values of J_{sym} (e.g. negative values of J_{sym}) lead to super-soft symmetry energies. The system then becomes very neutron-rich with $\delta \approx 1$ at high densities. In this case, as shown in Figure 2, the symmetry energy decreases with increasing density, giving a negative contribution (the second term in Eq. 2) to the total pressure. To support the same NSs as massive as $1.97 M_{\odot}$ or even $1.4 M_{\odot}$, a much larger contribution to the total pressure from the symmetric part ($E_0(\rho)$ term) is thus required. Because of the weaker correlation between K_0 and the data/conditions used, as shown in Figure 5, it is the J_0 that dominates the contribution to the high-density pressure from the $E_0(\rho)$ term. Therefore, the value of J_0 has to be positive when J_{sym} is very small. This conclusion can also be seen in Figure 10 of ref. (Zhang & Li 2019a) where the constant surface of the maximum mass $2.01 M_{\odot}$ was examined in the 3-dimensional J_0 - K_{sym} - J_{sym} high-density EOS parameter space. We note here that such features were not seen in other Bayesian analyses because the $E_{\text{sym}}(\rho)$

Table 4. 68%, 90% Credible Intervals and most probable values of the symmetry energy $E_{\text{sym}}(\rho)$

ρ/ρ_0	90% Lower Limit	68% Lower Limit	Most Probable	68% Upper Limit	90% Upper Limit
1.0	29.2	30.8	34.0	34.8	34.8
1.1	30.3	32.0	35.2	36.7	37.0
1.2	31.1	32.8	36.1	38.4	39.2
1.3	31.5	33.4	36.9	40.0	41.3
1.4	31.7	33.7	37.5	41.6	43.4
1.5	31.5	33.8	37.9	43.1	45.6
1.6	31.1	33.6	38.3	44.7	47.9
1.7	30.3	33.2	38.5	46.2	50.2
1.8	29.3	32.6	38.8	47.8	52.7
1.9	28.0	31.9	38.9	49.5	55.3
2.0	26.4	31.0	39.2	51.3	58.2
2.1	24.6	29.9	39.4	53.2	61.2
2.2	22.5	28.7	39.7	55.3	64.5
2.3	20.2	27.4	40.2	57.6	68.1
2.4	17.7	26.0	40.7	60.2	72.0
2.5	14.9	24.5	41.4	63.0	76.2
2.6	11.9	22.9	42.3	66.0	80.8
2.7	8.6	21.3	43.4	69.5	85.8
2.8	5.2	19.6	44.8	73.2	91.2
2.9	1.6	18.0	46.4	77.3	97.1
3.0	-2.3	16.3	48.4	81.9	103.4

was not allowed to become super-soft *a priori* by setting $J_{\text{sym}}=0$, or often the isospin-independent polytropic EOSs are used at high densities.

It is also interesting to see that there is a small shoulder for the PDF of K_{sym} around $K_{\text{sym}} \approx -100$ MeV. This is also because of the correlations among J_0 , J_{sym} and K_{sym} . As shown in Figure 4, when J_0 has values in the region of 0~200 MeV, J_{sym} has negative values while K_{sym} has values of about -100 MeV with appreciably higher probabilities than the surrounding area on the contour plots of the correlations.

3.2. The Bayesian inferred high-density EOS confidence intervals

After obtaining the most probable values and the quantified uncertainties for the EOS parameters, one can derive the corresponding EOS according to Eqs. (5) and (6). Show in Figure 1 are the symmetry energy $E_{\text{sym}}(\rho)$ and the nucleon specific energy $E_0(\rho)$ in SNM as functions of the reduced density ρ/ρ_0 . They are also tabulated with their corresponding 90% and 68% confidence ranges in Table 4 and Table 5, respectively.

In Figure 1, the black, blue and red shadows represent the prior, 90% and 68% credible areas, respectively. As mentioned in the introduction, both the $E_{\text{sym}}(\rho)$ and $E_0(\rho)$ are constrained into narrow bands at densities smaller than about $2.5\rho_0$. However, the symmetry energy diverges broadly at higher densities because of the poor constraint on J_{sym} . More quantitatively, the symmetry energy at $2\rho_0$ is found to be $E_{\text{sym}}(2\rho_0) = 39.2^{+12.1}_{-8.2}$ MeV at 68% confidence level as shown in Table 4. This value is consistent with the values extracted very recently from several other studies albeit not always with quantified uncertainties. For example, $E_{\text{sym}}(2\rho_0) = 46.9 \pm 10.1$ MeV at 100% confidence level was found in ref. (Zhang & Li 2019a) by inverting several NS observables in the 3-dimensional J_0 - K_{sym} - J_{sym} high-density EOS parameter space while all other low-order parameters are fixed at their currently known most probable values. While this comparison is somewhat unfair because of the different assumptions and methods used, the general agreement is encouraging. Interestingly, an upper bound of 53.2 MeV was derived very recently in ref. (Tong et al. 2019) by studying the radii of neutron drops using the state-of-the-art nuclear energy density functional theories. In addition, $E_{\text{sym}}(2\rho_0) \in [39.4^{+6.4}_{-7.5}, 54.5^{+3.2}_{-3.1}]$ MeV was found from combined analyses of several NS observables and terrestrial laboratory data (Zhou et al. 2019). The value of $E_{\text{sym}}(2\rho_0)$ we inferred also falls well within the range of about 26~66 MeV from the Bayesian analyses of ref. (Baillot et al. 2019). Moreover, in a recent study of cooling

Table 5. 68%, 90% Credible Intervals and most probable values for the SNM EOS $E_0(\rho)$

ρ/ρ_0	90% Lower Limit	68% Lower Limit	Most Probable	68% Upper Limit	90% Upper Limit
1.0	-16.0	-16.0	-16.0	-16.0	-16.0
1.1	-15.9	-15.9	-15.9	-15.9	-15.9
1.2	-15.5	-15.5	-15.5	-15.5	-15.4
1.3	-14.9	-14.9	-14.9	-14.8	-14.7
1.4	-14.1	-14.1	-14.1	-13.9	-13.8
1.5	-13.1	-13.1	-13.1	-12.7	-12.5
1.6	-11.9	-11.9	-11.8	-11.2	-11.0
1.7	-10.6	-10.4	-10.4	-9.6	-9.2
1.8	-9.0	-8.8	-8.7	-7.7	-7.2
1.9	-7.3	-7.0	-6.9	-5.5	-4.9
2.0	-5.5	-5.1	-4.8	-3.1	-2.4
2.1	-3.5	-3.0	-2.6	-0.6	0.4
2.2	-1.3	-0.7	-0.3	2.2	3.4
2.3	0.9	1.7	2.3	5.3	6.6
2.4	3.3	4.3	5.0	8.5	10.1
2.5	5.7	7.0	7.8	11.9	13.8
2.6	8.2	9.8	10.8	15.5	17.8
2.7	10.8	12.7	13.9	19.3	21.9
2.8	13.5	15.7	17.1	23.2	26.3
2.9	16.2	18.8	20.5	27.4	30.9
3.0	19.0	22.0	24.0	31.7	35.7
3.1	21.8	25.2	27.5	36.2	40.7
3.2	24.6	28.6	31.2	40.8	45.9
3.3	27.5	32.0	35.0	45.6	51.3
3.4	30.3	35.4	38.8	50.6	56.9
3.5	33.1	38.9	42.8	55.6	62.6
3.6	35.9	42.4	46.8	60.9	68.6
3.7	38.7	46.0	50.8	66.2	74.7
3.8	41.4	49.5	54.9	71.7	81.0
3.9	44.1	53.1	59.1	77.3	87.5
4.0	46.7	56.7	63.3	83.0	94.2

timescales of protoneutron stars (Nakazato & Suzuki 2019), the $E_{\text{sym}}(2\rho_0)$ was used as a controlling parameter in constructing a series of phenomenological EOS models. It was found that EOS modes with $E_{\text{sym}}(2\rho_0)=40\sim 60$ MeV can account for the NS radius and tidal deformability indicated by GW170817. Overall, results from all of these studies are in general agreement within the still relatively large uncertainties.

At this point, it is useful to note that constraining the $E_{\text{sym}}(\rho)$ at supra-saturation densities has been a longstanding goal of the low-intermediate energy heavy-ion reaction community. However, current results on the $E_{\text{sym}}(2\rho_0)$ based on existing data from heavy-ion reactions with stable beams are still inconclusive (Li et al. 2019; Trautmann 2019). Quantitatively, the 68% confidence upper boundary of $E_{\text{sym}}(2\rho_0)$ inferred in this work overlaps with the 100% confidence lower boundary of the $E_{\text{sym}}(2\rho_0)$ extracted by the ASY-EOS Collaboration from analyzing their data on the relative flows of neutrons with respect to (w.r.t) protons, tritons w.r.t. ^3He and yield ratios of light isobars (Russotto et al. 2011, 2016). Our results, however, is significantly above the super-soft $E_{\text{sym}}(2\rho_0)$ preferred by some transport model analyses of the earlier data on the charged pion ratio (Xiao et al. 2009). Hopefully, ongoing and planned new experiments especially with high-energy radioactive beams at several advanced rare isotope beam facilities together with improved analysis tools more systematically tested by the broad reaction community will provide more rigorous terrestrial constraints on the $E_{\text{sym}}(\rho)$ at supra-saturation densities. Then, a much more meaningful

comparison of the high-density nuclear symmetry energy functionals extracted from astrophysical observations and terrestrial experiments can be made.

As discussed earlier, the J_0 parameter has the strongest influence on the maximum mass of neutron stars. Because of the sharp cut-off at $1.97 M_\odot$ used in the default calculations, the PDF of J_0 is rather focused. Consequently, as shown in the lower panel of Figure 1, the $E_0(\rho)$ in SNM is well constrained up to about $4\rho_0$. More quantitatively, $E_0(4\rho_0)=63.3^{+19.7}_{-6.6}$ MeV at 68% confidence level, as shown in Table 5. In a recent study (Zhang & Li 2019c), influences of the recently reported mass $M=2.17^{+0.11}_{-0.10} M_\odot$ of PSR J0740+6620 on the EOS of neutron-rich nuclear matter were analysed. It was found that this new maximum mass of NSs can raise the lower limit of J_0 from about -220 MeV to -150 MeV. It provides a tighter constrain on the EOS of neutron-rich nucleonic matter, especially its symmetric part $E_0(\rho)$. This point is verified by the present work as we shall discuss in the next section.

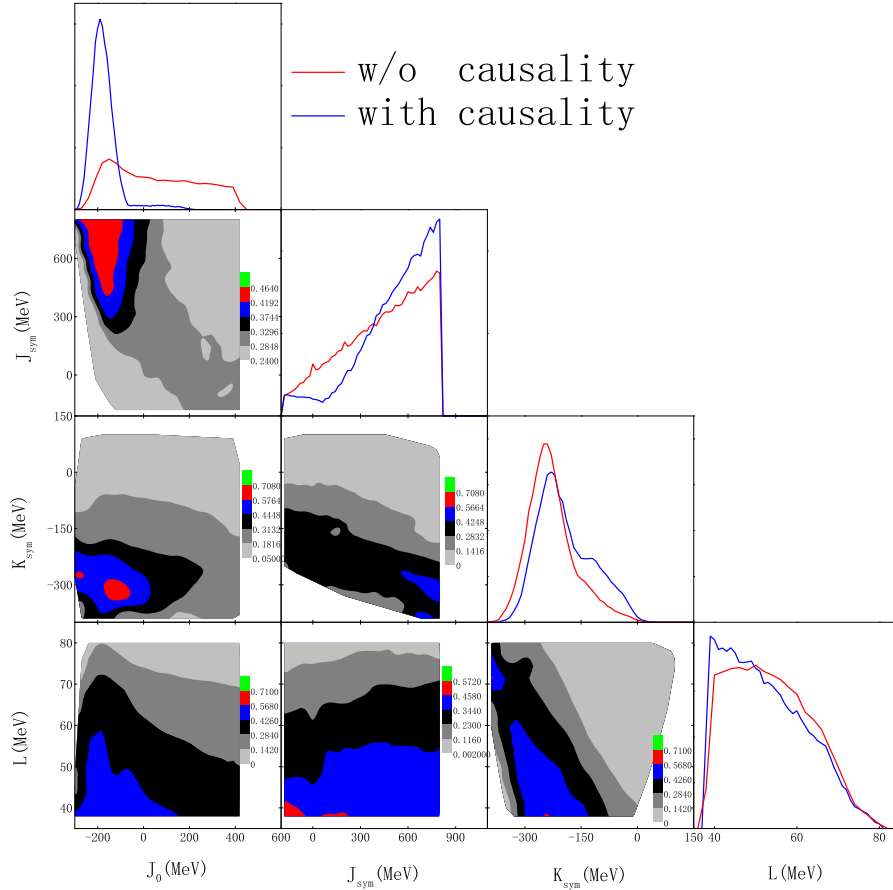


Figure 7. Posterior probability distribution functions of high-density EOS parameters with and without requiring the causality condition. The correlation contours are for the case without enforcing the causality condition.

4. INDIVIDUAL ROLES OF KEY MODEL INGREDIENTS AND NEUTRON STAR DATA IN BAYESIAN INFERENCE OF THE HIGH-DENSITY EOS PARAMETERS

As we discussed earlier, different ways of parameterizing the EOS have been used in the literature. In particular, not all isospin-dependent parameterizations use simultaneously both the J_0 and J_{sym} terms. How does this different treatment affects what we extract from the same data the high-density behavior of nuclear EOS? Thanks to the continuing great efforts in astronomy, a new record of the maximum mass of NSs may be set at anytime. How does the variation of the NS maximum mass affect what we extract from the same radius data the high-density behavior of nuclear EOS? In addition, it has been pointed out that whether one use a sharp-cut off or a Gaussian function for the

NS maximum mass may affect significantly what one can infer from the Bayesian analyses (Miller et al. 2019). How does this affect what we learn about the high-density behavior of nuclear EOS? Moreover, we have a dream: the $R_{1.4}$ of canonical NSs has just been measured to better than 5% 1σ statistical accuracy with no disagreement from different observations and/or analyses. How does this dreamed case help improve our knowledge about the EOS compared to the default calculations in the previous section? In the following, we discuss results of our studies on these questions.

4.1. The role of causality condition

The causality condition requires that the speed of sound, defined by $v_s^2 = dP/d\epsilon$, should not exceed the speed of light, namely, $0 \leq v_s^2 \leq c^2$. This condition naturally limits some of the EOS parameters through the pressure P and the energy density ϵ . While to our best knowledge there is no disagreement about whether the causality condition should be enforced or not, it is educational and interesting to compare results obtained with and without enforcing the causality condition. At least, it allows us to check if our Bayesian inference code does what it is supposed to do. Moreover, we can learn which parameters are mostly affected by the causality condition.

Shown in Figure 7 are the posterior PDFs of high-density EOS parameters with or without considering the causality condition. The correlation contours are obtained without using the causality condition. Compared to the PDFs obtained with causality, a wider range extending to large positive values of J_0 with higher probabilities is now allowed. This is simply because the causality condition sets the absolute upper limit of the NS maximum mass and consequently the upper limit of J_0 . Without enforcing the causality condition, the most stringent constraint on J_0 now comes from the requirement to support NSs at least as massive as $1.97 M_\odot$. However, this only sets a lower limit for J_0 while its upper limit has been removed. Because of its anti-correlation with J_0 , the parameter J_{sym} now has higher probabilities to be small when the J_0 has higher probabilities to be large. It is also worth noting that the small peak for the PDF of K_{sym} at about -100 MeV disappears now. Different from the correlations among J_{sym} , K_{sym} and J_0 shown in Figure 4, due to the larger and almost the same probability for J_0 in the range of $0 \text{ MeV} \leq J_0 \leq 400 \text{ MeV}$, the corresponding J_{sym} has the same probability in the range of $-200 \text{ MeV} \leq J_0 \leq 0 \text{ MeV}$. This makes the small shoulder in the PDF of K_{sym} disappear when the causality condition is switched off. As shown by the blue curves in Figure 7, both the J_{sym} and K_{sym} obtain higher probabilities to have higher values when the causality condition is turned on. Consequently, the high-density symmetry energy becomes stiffer when the causality condition is enforced. We also notice that the causality as a high-density condition has little effect on the PDFs of L and the low-order parameters as one expects.

4.2. The role of J_0 parameter of high-density SNM EOS

The high-order parameter J_0 characterizes the high-density behavior of the SNM EOS $E_0(\rho)$. To examine its role, shown in the left panels of Figure 8 are the PDFs of J_{sym} , K_{sym} and L when the parameter J_0 is fixed at 0, -180 and -220 MeV, respectively. For comparisons, the PDFs (grey lines) for them in the default case with J_0 in the range of -800 to 400 MeV shown in Figure 4 are also included. It is seen that the J_0 has significant effects on the PDFs of J_{sym} and K_{sym} , but less influences on the PDF of L . The effects of J_0 on the parameters K_0 and $E_{\text{sym}}(\rho_0)$ are very weak and thus not shown here. As shown in Figure 4, because of the negative (positive) correlations between J_0 and J_{sym} (K_{sym}), an increase of J_0 leads to a decrease of J_{sym} but an increase of K_{sym} . It is interesting to note that the J_{sym} becomes completely negative when the J_0 is set to zero. This is understandable by noticing that the most probable value of J_0 is -190 MeV in the default case as shown in Table 3. Artificially setting $J_0=0$ is equivalent to making the SNM EOS super-stiff with a much higher contribution to the total pressure. Then, to meet the same conditions especially the maximum mass and causality constraints, the contribution to the pressure from the symmetry energy has to be significantly reduced by making the J_{sym} largely negative to cancel out the increase of the pressure due to the effectively large increase in J_0 . On the other hand, it is known that the radius of canonical NSs is almost independent of J_{sym} , while to maintain the same radius the K_{sym} and L have to be anti-correlated as shown in Fig. 7 of ref. (Zhang & Li 2019b). It is thus also easy to understand that while the peak of the PDF of K_{sym} is shifted from about -230 MeV to -50 MeV, the PDF of L shifts appreciably towards smaller L values.

Overall, when the NS radii data and the maximum mass are used to infer nuclear symmetry energy, whether to keep a J_0 term and what is its uncertainty range all play particularly important roles in determining especially the PDFs of J_{sym} and K_{sym} , namely the high-density behavior of nuclear symmetry energy. Shown in the right panels of Figure 8 are the 68% CFL boundaries of the symmetry energy and the nucleon specific energy $E_0(\rho)$ in SNM as a function of reduced density with $J_0=0, -180, -220 \text{ MeV}$, respectively. For comparisons, the default results from Figure 1 are also included. The following observations can be made: (1) The symmetry energy obtained with a constant of $J_0=-180 \text{ MeV}$ (which is very close to the most probable value of -190 MeV in the default case as shown in Table 3) is close to the one in the default calculation using $J_0=-800 \text{ MeV} \sim 400 \text{ MeV}$; (2) Below about $2.5\rho_0$, except the case with

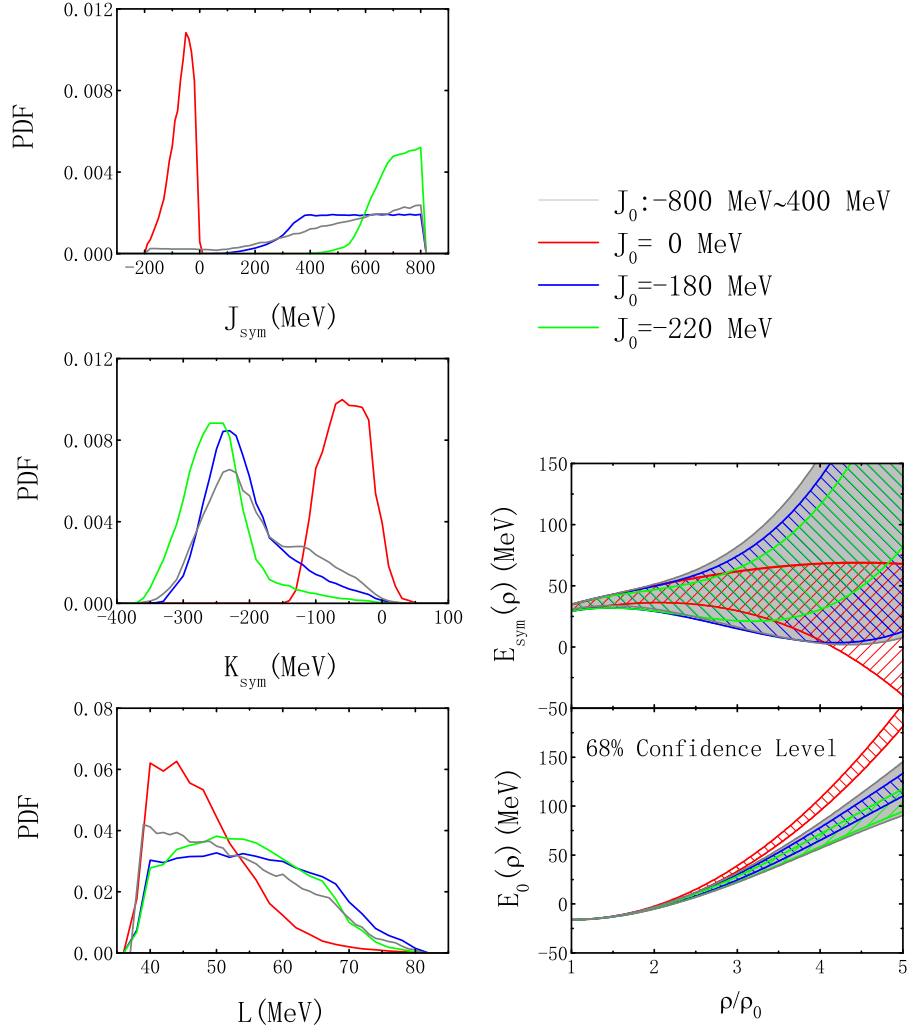


Figure 8. Left: Posterior probability distribution functions of high-density EOS parameters by setting the parameter J_0 to 0, -180 and -220 MeV, respectively. Right: The role of J_0 parameter on inferring the high-density symmetry energy and nucleon specific energy $E_0(\rho)$ in SNM.

$J_0=0$ MeV, both the $E_{\text{sym}}(\rho)$ and $E_0(\rho)$ are almost independent of the J_0 value; (3) The value of J_0 is important for understanding the EOS at densities higher than about $3\rho_0$.

4.3. The role of J_{sym} parameter of high-density symmetry energy

The parameter J_{sym} describes the behavior of nuclear symmetry energy at densities higher than about $2\rho_0$, as shown in the right panels of Figure 2. As noted above, the parameter J_{sym} is less constrained by the present $R_{1.4}$ radius data because the average density reached in canonical neutron stars are not so high, and it is known that the radius of canonical NSs is most sensitive to the pressure around $2\rho_0$. As mentioned earlier, in some studies for various purposes in the literature, the parameter J_{sym} is often set to zero, namely, parameterizing the symmetry energy up to ρ^2 only. Therefore, it is useful to study effects of varying J_{sym} on the PDFs of high-density EOS parameters within the framework of this work. As we shall see next, effects of J_{sym} can be explained similarly as those of J_0 using the same correlations among the high-density EOS parameters.

Shown in the left panels of Figure 9 are the PDFs for J_0 , K_{sym} and L with $J_{\text{sym}}=0, 300, 800$ MeV, respectively. For comparisons, the PDFs for them from the default calculation (grey lines) using J_{sym} between -200 MeV and 800 MeV

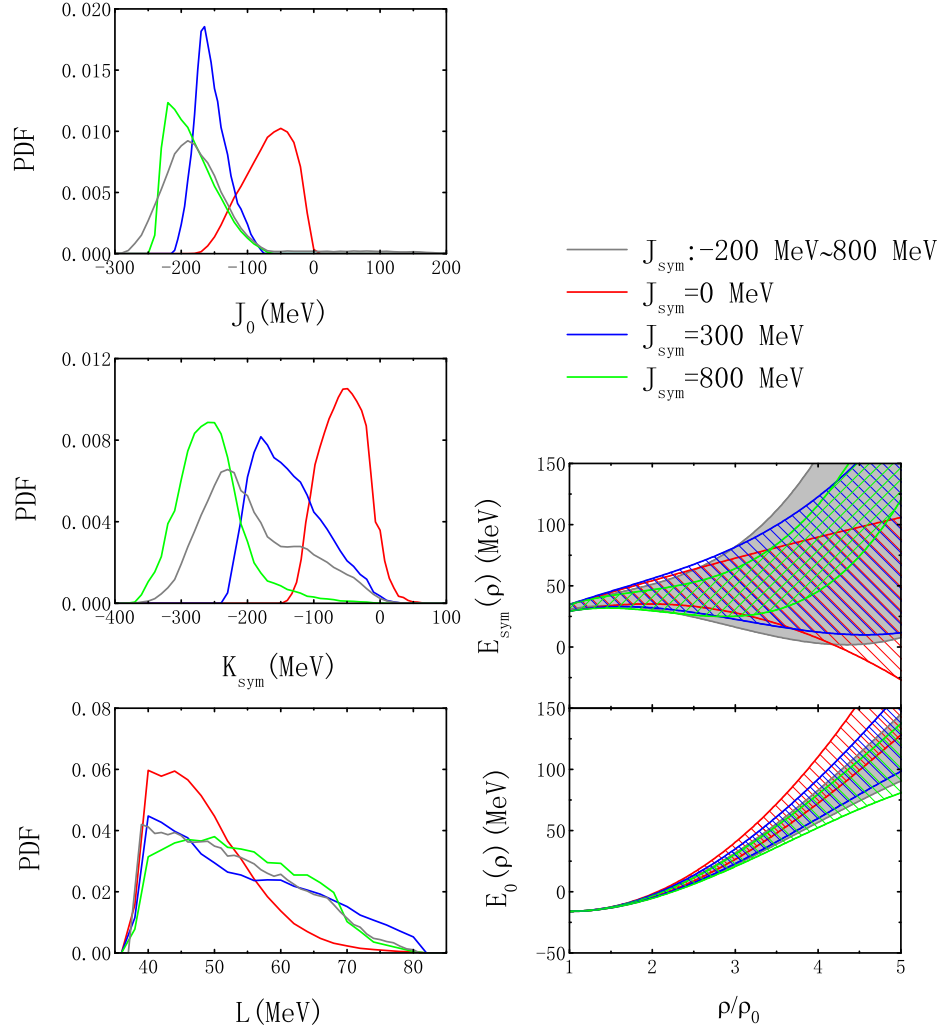


Figure 9. Left: Posterior probability distribution functions of high-density EOS parameters by fixing J_{sym} at 0, 300 and 800 MeV, respectively. Right: The corresponding effects on inferring the high-density symmetry energy and nucleon specific energy $E_0(\rho)$ in SNM.

are also included. The PDFs of K_0 and $E_{\text{sym}}(\rho_0)$ are not given here because of their weaker correlations with J_{sym} . It is seen that the J_0 is always negative when positive values of J_{sym} are taken. It implies that the contribution to the pressure from the $E_{\text{sym}}\delta^2$ term in Eq. (2) with positive J_{sym} values is high enough that the required contribution from the SNM EOS $E_0(\rho)$ term is smaller. Both J_0 and K_{sym} become larger as J_{sym} decreases because of the negative correlations between J_{sym} and J_0 , as well as between J_{sym} and K_{sym} . While the variation of J_{sym} has less influences on the PDF of L .

We notice again that the most probable values of J_0 and J_{sym} are -190 MeV and 800 MeV, respectively, in the default calculation. Setting J_{sym} to zero requires a significant increase of J_0 , leading to a much stiffer EOS for SNM at densities higher than about $2.5\rho_0$. This is clearly seen in the lower right panel of Figure 9 where the 68% CFL boundary of SNM EOS with the fixed J_{sym} values are shown. The default results from Figure 1 are also shown for comparisons. The EOS of SNM becomes softer at densities higher than $2.5\rho_0$ as J_{sym} increases. This is due to the fact that J_0 becomes small with increasing values of J_{sym} , while the K_0 is weakly correlated to J_{sym} . Except the extreme case with $J_{\text{sym}} = 800 \text{ MeV}$, both the $E_{\text{sym}}(\rho)$ and $E_0(\rho)$ are almost independent of J_{sym} at densities below about $2.5\rho_0$. For the $E_{\text{sym}}(\rho)$, the default calculation and the calculations with the fixed J_{sym} values largely overlap up to

about $5\rho_0$. In particular, the symmetry energy at high densities does not become much stiffer when the fixed value of J_{sym} increases. This is because the value of K_{sym} automatically becomes smaller as J_{sym} increases due to their anti-correlation.

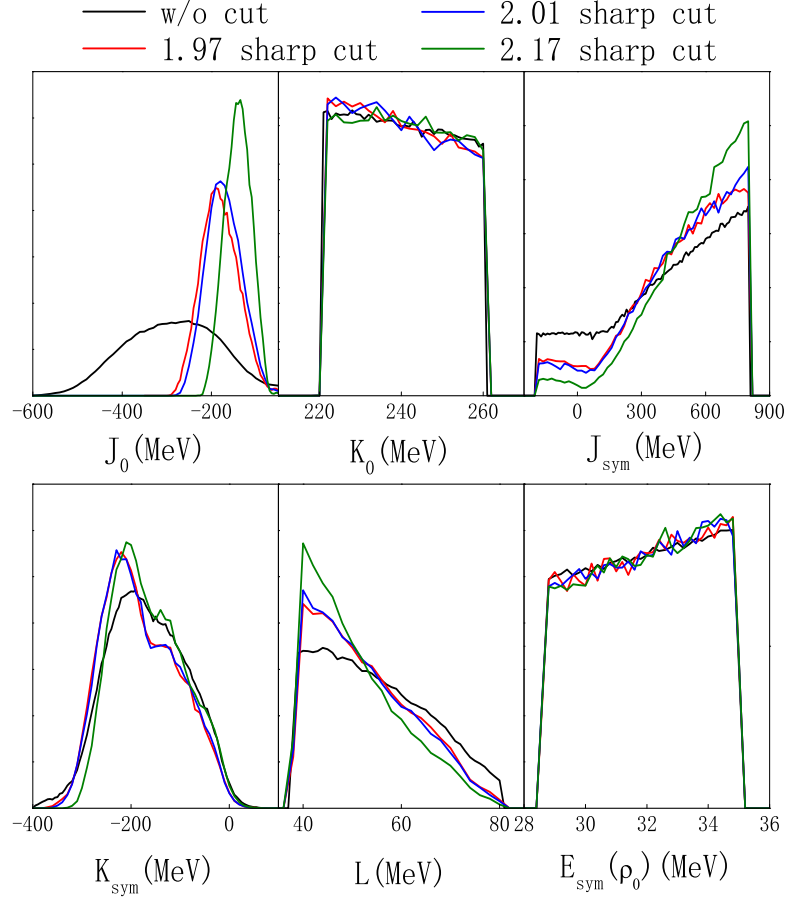


Figure 10. Posterior probability distribution functions of EOS parameters from calculations without a lower limit and with a sharp cut-off at 1.97, 2.01 and 2.17 M_\odot for the NS maximum mass, respectively.

More comments on the case with $J_{\text{sym}}=0$ are necessary. This option has been used in many studies in the literature, see, e.g. refs. (Alam 2014; Baillot et al. 2019). The PDFs for J_0 , K_{sym} and L as well as their correlations in this case have been shown already in Figure 6. As we noticed earlier, setting $J_{\text{sym}}=0$ leads to the anti-correlation between J_0 and K_{sym} consistent with the result in ref. (Baillot et al. 2019) but contrary to our default results shown in Figure 4. This difference has some important consequences. For example, the value of $J_0 = -50^{+40}_{-80}$ MeV at 68% CFL is inferred from the present study while $J_0 = 318^{+673}_{-366}$ MeV was obtained in ref. (Baillot et al. 2019). On the other hand, the values of $K_{\text{sym}} = -50^{+40}_{-70}$ MeV and $L = 44^{+16}_{-6}$ MeV at 68% CFL we inferred by setting $J_{\text{sym}}=0$ are consistent with the results in ref. (Baillot et al. 2019). Consistent with our conclusions about the role of J_0 in inferring the EOS of dense neutron-rich matter, while setting $J_0 = 0$ affects significantly the accuracy of inferring the high-density symmetry energy, setting $J_{\text{sym}}=0$ affects significantly the accuracy of inferring the high-density EOS of SNM, because of the strong anti-correlation between the J_0 and J_{sym} parameters.

4.4. The role of the observed maximum mass of neutron stars in constraining the high-density EOS

As mentioned earlier, the maximum mass of NSs is considered as an observable in this work. Since the maximum mass is still changing as more extensive and accurate observations are being made, it is interesting to examine how the value and the way the NS maximum mass information is used may affect what we learn about the high-density

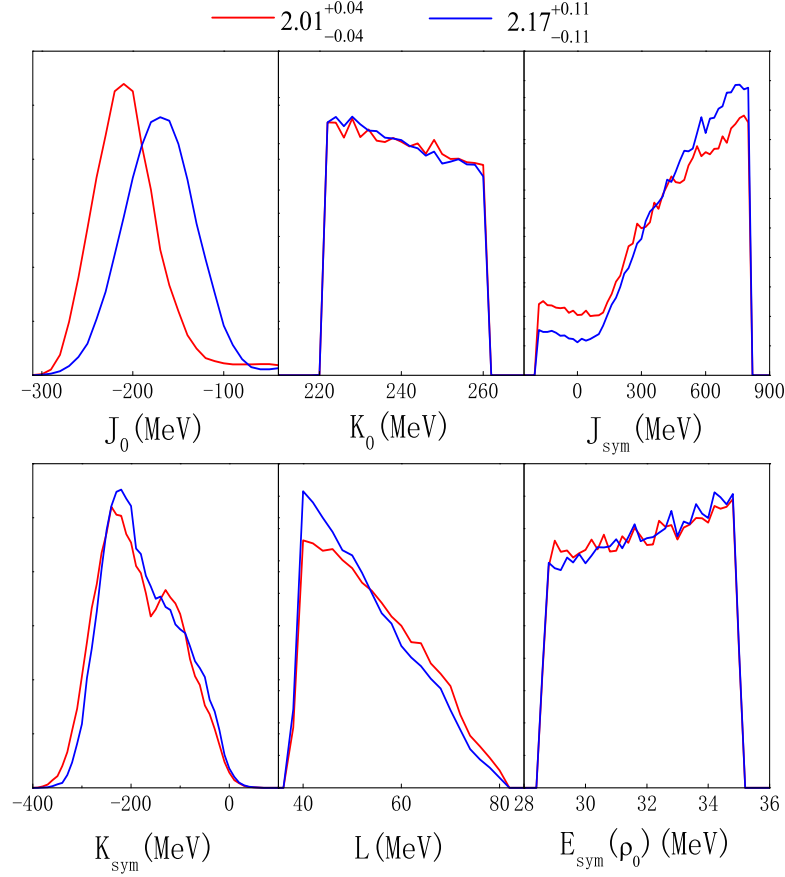


Figure 11. Posterior probability distribution functions of EOS parameters from calculations with a Gaussian distribution centered at 2.01 and 2.17 M_{\odot} , respectively, for the NS maximum mass.

EOS from Bayesian inferences. For this purpose, we compare results of the following calculations with the default results: (i) Without requiring a lower limit for the maximum mass (referred as the NS minimum maximum mass in the following) the EOSs have to support; (ii) With a sharp cut-off at 1.97, 2.01 and 2.17 M_{\odot} , respectively, for the minimum maximum mass; (iii) The minimum maximum mass is a Gaussian distribution centered at 2.01 and 2.17 M_{\odot} with a 1σ width of 0.04 M_{\odot} and 0.11 M_{\odot} , respectively.

Shown in Figure 10 are the PDFs of the EOS parameters from the cases (i) and (ii). Obviously and easily understood, the lower limit of J_0 has to go up to support gradually more massive NSs while its upper limit remains the same. Consequently, the most probable value of J_0 increases, leading to more stiff SNM EOS as shown in Figure 12. It is interesting to see that the PDF of J_{sym} shifts to favor higher J_{sym} values, leading to an increased mean value of the latter when the NS minimum maximum mass increases from 1.97 to 2.17 M_{\odot} . Namely, now the mean values of both J_0 and J_{sym} increase seemingly in contradiction with their anti-correlation observed in the default calculation where the NS minimum maximum mass is fixed at 1.97 M_{\odot} . This is easily understandable because the maximum pressure is no longer the same in calculations with different NS minimum maximum masses. Contributions to the increased pressure necessary to support more massive NSs can come from both the high-density SNM EOS and symmetry energy. As a result, the mean values of both J_0 and J_{sym} increase as the NS minimum maximum mass increases, while effects on other EOS parameters are weak. Thus, as demonstrated recently in ref. (Zhang & Li 2019c), more precise measurements of the NS maximum mass will improve our knowledge about the high-density behavior of both SNM EOS and nuclear symmetry energy. The same phenomena are observed when the Gaussian distributions are used for the minimum maximum mass as shown in Figure 11 for the case (iii). As indicated, one minimum maximum mass distribution centers at 2.01 M_{\odot} with a 1σ width of 0.04 M_{\odot} , while the other one centers at 2.17 M_{\odot} with a 1σ width

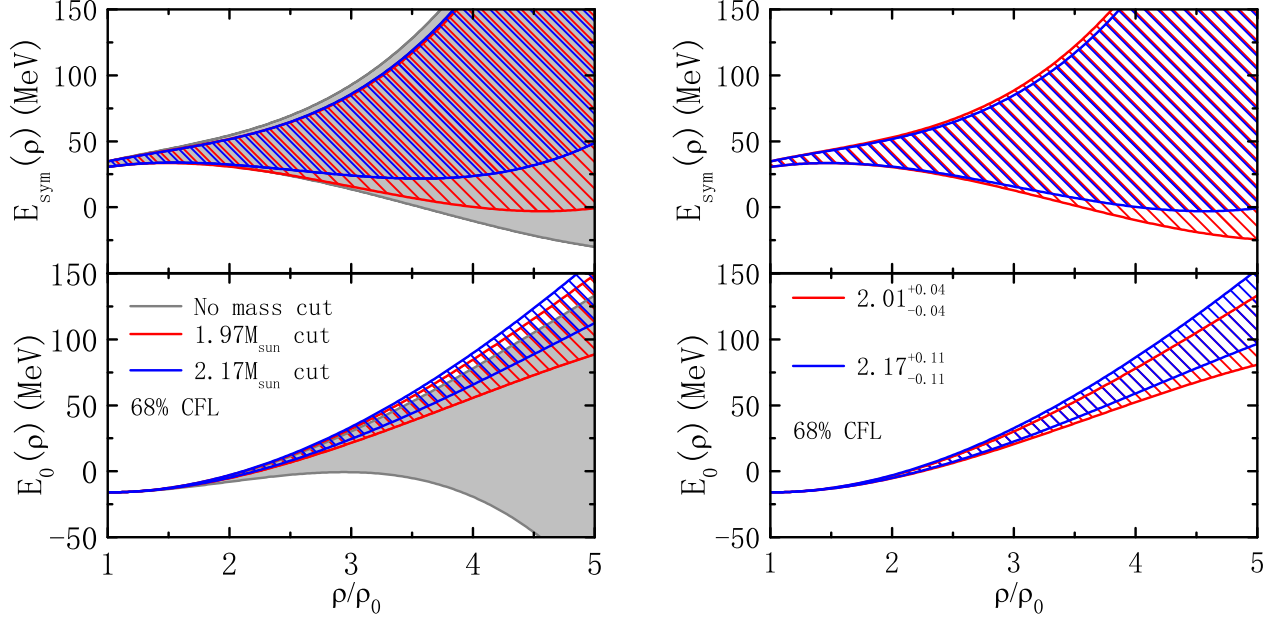


Figure 12. Effects of using different NS minimum maximum masses on the high-density symmetry energy and nucleon specific energy $E_0(\rho)$ in SNM at 68% CFL.

of $0.11 M_\odot$. The PDFs of both J_0 and J_{sym} shift towards higher J_0 and J_{sym} values as the central mass increases from 2.01 to $2.17 M_\odot$. Again, this is easily understood.

Effects of using different NS minimum maximum masses on the high-density symmetry energy and nucleon specific energy $E_0(\rho)$ in SNM at 68% CFL are shown in Figure 12. The following observations can be made: (1) The maximum mass condition plays an increasingly more appreciable role in determining the symmetry energy only at densities higher than about $2.5\rho_0$. A higher value for the NS minimum maximum mass raises the lower limit for the high-density symmetry energy mainly due to the increased mean value of J_{sym} as we just discussed above, while the upper limit does not change much; (2) The maximum mass condition has a significant impact on the SNM EOS at $\rho > 2\rho_0$. The increased NS maximum mass requires higher values of J_0 while the saturation parameters are basically not affected, stiffening the SNM EOS above about $2\rho_0$; (3) As shown in the right panels of Figure 12, using the two different Gaussian distributions for the NS minimum maximum mass does not cause any obvious change in the high-density EOS compared to the calculations with the sharp cut-offs. Of course, the two different central masses have some obvious and easily understood effects. We emphasize that this is probably due to the fact that the radius data we used is only for a single NS of mass $1.4 M_\odot$ instead of a group of NSs involving more massive ones.

4.5. The role of $R_{1.4}$ measurement accuracy on symmetry energy parameters

Here we study how much better we can infer the EOS parameters by using the two sets of imaginary data given in Table 1. The imaginary case-1 contains three data points with mean radii different from each other by about 1 km (i.e., a 10% systematic error) but the same absolute error bar of 0.8 km at 90% CFL. The average radius of this case is 11.5 km. While the imaginary case-2 has a single radius of 11.9 km and the same statistical error bar of 0.8 km as in the case-1. The PDFs of EOS parameters from these two imaginary cases are compared with those from our default calculations in Figure 13. It is seen that the case-1 and our default calculations give essentially the same PDFs for all six EOS parameters. Although in case-1, the statistical error is smaller compared to the default case, since the mean radii of the three points are already different by about 1 km, it is not surprising that the PDFs of case-1 are not much different from the default case. The PDFs of the imaginary case-2 are appreciably different from those of the default case, especially for K_{sym} and L . More quantitatively, as listed in Table 6, the most probable values of both K_{sym} and L increase significantly while their 68% CFL ranges remain approximately the same as the imaginary case-1 or the default case. In addition, the mean value of J_0 slightly increases while the mean value of J_{sym} decrease slightly.

Without changing any other conditions, the increase of mean radius from about 11.5 km in the default case to 11.9 km in the imaginary case-2 requires an increase in pressure around $2\rho_0$ while keeping the pressures at high density

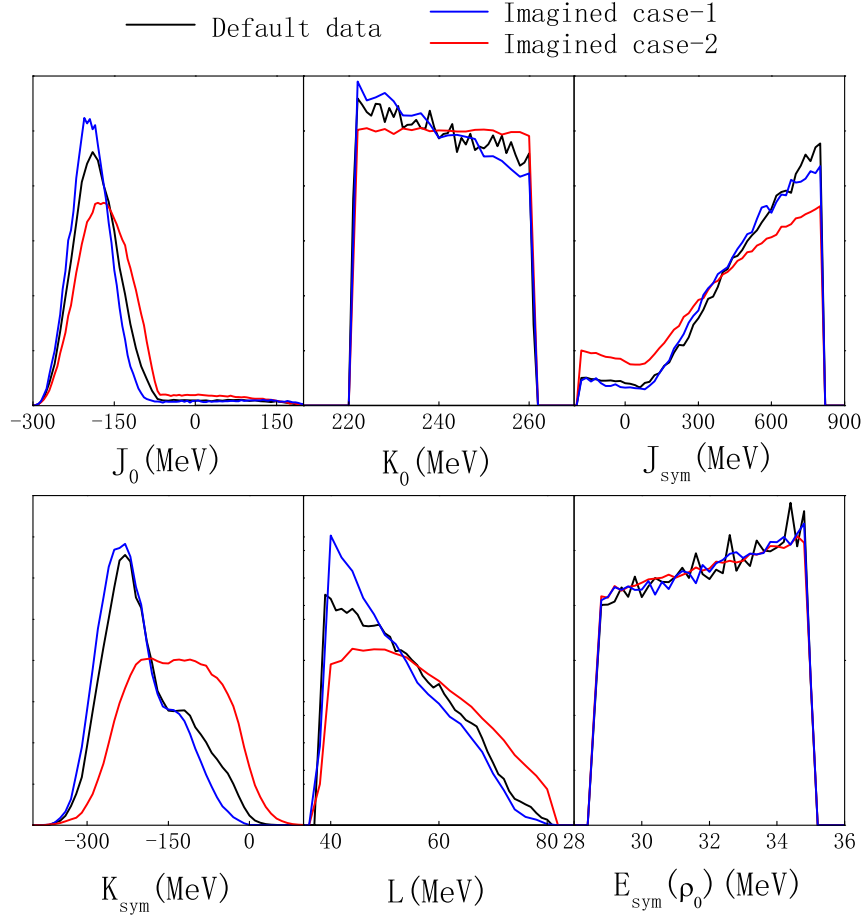


Figure 13. Effects of different precisions of measuring $R_{1.4}$ shown in Table 1 on the PDFs of EOS parameters.

Table 6. Most probable values of the EOS parameters and their 68% CFL boundaries obtained using the imagined data listed in Table 1.

Quantity	Imagined case-1	Imagined case-2
J_0	-190^{+30}_{-40}	-170^{+50}_{-50}
K_0	232^{+14}_{-12}	236^{+16}_{+12}
J_{sym}	800^{+20}_{-340}	800^{+0}_{-440}
K_{sym}	-240^{+70}_{-50}	-180^{+130}_{-40}
L	40^{+16}_{-2}	44^{+18}_{-6}
$E_{\text{sym}}(\rho_0)$	$33.8^{+1.0}_{-3.2}$	$34.6^{+0.2}_{-4.0}$

approximately the same to satisfy the same condition on the maximum mass. The increase in pressure around $2\rho_0$ can be achieved by increasing the K_0 , J_0 and/or L and K_{sym} . While an increase in J_0 normally leads to a decrease in J_{sym} as we discussed earlier due to the maximum mass constraint at high densities. Thus, the observed variations of the PDFs can all be qualitatively understood. Quantitatively, however, reducing the statistical and removing the systematic error bars in measuring the $R_{1.4}$ does not seem to help narrow down the PDFs of the EOS parameters compared to the default calculation using the real data. While we probably just made up bad numbers in our otherwise very good dream, this finding may be disappointing but not surprising. Our study here using only the radius data of a single canonical NS sets a useful reference. In reality, joint PDFs of the mass-radius measurements are normally inferred from Bayesian analyses of the raw data from observations. A collection of such data extending to heavy mass

regions, or the high precision radius data of several NSs with different masses will certainly help put much tighter bounds on the PDFs of the high-density EOS parameters. Our preliminary studies using several different hypothetical mass-radius correlations between 1.2 to 2 M_\odot indicate that they lead to very different PDFs of EOS parameters. Results of this study will be reported elsewhere.

5. SUMMARY AND OUTLOOK

In summary, using an explicitly isospin-dependent parametric EOS of nucleonic matter we carried out a Bayesian inference of high-density nuclear symmetry energy $E_{\text{sym}}(\rho)$ and the associated nucleon specific energy $E_0(\rho)$ in SNM using the latest $R_{1.4}$ radius data available in the literature, under several general conditions required for all NS models. The most important physics findings from this study are

- The available astrophysical data can already improve significantly our knowledge about the $E_0(\rho)$ and $E_{\text{sym}}(\rho)$ in the density range of $\rho_0 - 2.5\rho_0$ compared to what we currently know about them based mostly on terrestrial nuclear experiments and predictions of nuclear many-body theories. In particular, the symmetry energy at $2\rho_0$ is determined to be $E_{\text{sym}}(2\rho_0) = 39.2^{+12.1}_{-8.2}$ MeV at 68% CFL approximately independent of the EOS parameterizations used and uncertainties of the absolutely maximum mass of NSs. However, at higher densities, the 68% confidence boundaries for both the $E_0(\rho)$ and $E_{\text{sym}}(\rho)$ diverge depending strongly on the EOS parameterizations used and several uncertainties.
- A precise measurement of $R_{1.4}$ alone with less than 5% 1σ statistical error and no systematic error will not improve much the constraint on the EOS of neutron-rich nucleonic matter at densities below about $2.5\rho_0$ compared to the constraints extracted from using the available radius data. While we are hopeful that high precision joint PDFs from simultaneous mass-radius measurements extending to heavy mass regions will significantly further narrow down the EOS both below and above $2.5\rho_0$.
- The radius data and other general conditions, such as the observed NS maximum mass and causality condition introduce strong correlations for the high-order parameters used in parameterizing the $E_0(\rho)$ and $E_{\text{sym}}(\rho)$. Reflected clearly in the PDFs of the high-density EOS parameters, the high-density behavior of $E_{\text{sym}}(\rho)$ inferred depends strongly on how the high-density $E_0(\rho)$ is parameterized, and vice versa. This is particularly true for densities higher than about $2.5\rho_0$ where the third-order parameters J_0 and J_{sym} play the dominating role. Since these two parameters are not always used simultaneously in parameterizing the $E_0(\rho)$ and $E_{\text{sym}}(\rho)$ in the literature, different correlations among the PDFs of EOS parameters and thus different high-density behaviors of the symmetry energy may be inferred from the same set of NS observational data.
- The value of the observed NS maximum mass and whether it is used as a sharp cut-off for the minimum maximum mass or through a Gaussian distribution in the Bayesian analyses affect significantly the lower boundaries of $E_0(\rho)$ and $E_{\text{sym}}(\rho)$ only at densities higher than about $2.5\rho_0$. While the EOS constraints extracted in the density region of $\rho_0 - 2.5\rho_0$ are not influenced by the remaining uncertainties about the NS absolutely maximum mass.

Finally, we speculate that radii of more massive NSs and additional messengers especially those directly from NS cores or emitted during collisions between two NSs or heavy nuclei will be useful to further constrain the EOS of dense neutron-rich nuclear matter especially at densities higher than about $2.5\rho_0$.

We thank Drs. Nai-Bo Zhang and De-Hua Wen for helpful discussions and Dr. Matt Wood for providing us the high-performance computing resources used for carrying out this work. Wen-Jie Xie is supported in part by the China Scholarship Council and appreciates the productive research conditions provided to him at Texas A&M University-Commerce. BAL acknowledges the U.S. Department of Energy, Office of Science, under Award Number DE-SC0013702, the CUSTIPEN (China-U.S. Theory Institute for Physics with Exotic Nuclei) under the US Department of Energy Grant No. DE-SC0009971.

REFERENCES

- Abbott, B. P., et al. 2018, PhRvL, 121, 161101
- Alam, N., et al. 2014, Phys. Rev. C **90**, 054317
- Alvarez-Castillo, D., Ayriyan, A., Benic, S., Blaschke, D., Grigorian, H., & Typel, S. 2016, European Physical Journal A 52, 69.
- Antoniadis, J., et al. 2013, Science, 340, 448
- Athena: Advanced Telescope for High-ENergy Astrophysics, 2014 <http://sci.esa.int/athena/>
- Baillet d'Etivaux, N., Guillot, S., Margueron, J., Webb, N. A., Catelan, M., & Reisenegger, A. 2019, arXiv:1905.01081
- Baiotti, L. 2019, arXiv:1907.08534, Prog. in Part. and Nucl. Phys., to appear.
- Balantekin, A.B. et al. (FRIB Theory Alliance Steering Committee) 2014, Nuclear Theory at the Facility for Rare Isotope Beams (FRIB), Mod. Phys. Lett. A 29, 1430010
- Baldo, M., & Burgio, G.F. 2016, Prog. Part. Nucl. Phys. **91**, 203
- Baran, V., Colonna, M., Greco, V. & Di Toro, M. 2005, Phys. Rep. **410**, 335
- Baym, G., Bethe, H. A., & Pethick, C. J. 1971b, Nucl. Phys. A, 175, 225
- Bombaci, I., & Lombardo, U. 1991, Phys. Rev. C **44**, 1892
- Bogdanov, S. et al, 2019, arXiv:1903.04648v1
- Burgio, G.F., & Fantina, A.F. 2018, *The Physics and Astrophysics of Neutron Stars* (Astrophysics and Space Science Library Book 457), Springer.
- Cai, B. J., Fattoyev, F. J., Li, B.A., & Newton, W.G. 2015, Phys. Rev. C 92, 015802
- Cai, B. J., & Chen, L. W. 2017, Nucl. Sci. Tech., 28, 185
- Chen, L. W. 2011, Sci. China: Phys. Mech. Astron. 54, suppl. s124
- Danielewicz, P., Lacey, R., & Lynch, W. G. 2002, Science, 298, 1592
- De, S., Finstad, D., Lattimer, J. M., Brown, D. A., Berger, E. & Biwer, C. M. 2018, Phys. Rev. Lett., 121, 091102
- Ditoro, M. et al. 2010, J. Phys. G. 37, 083101
- Drago, A. et al., 2014, Phys. Rev. C 90, 065809
- Farine, M., Pearson, J. M., & Tondeur, F. 1997, Nucl. Phys. A, 615, 135
- Fonseca, E. et al. 2019, arXiv:1903.08194v1
- Garg, U., & Colò, G. 2018, Prog. Part. Nucl. Phys. **101**, 55
- Greif, S. K., Raaijmakers, G., Hebeler, K., Schwenk, A., & Watts, A. L. 2019, Mon. Not. R. Astron. Soc. 485, 5363
- Hastings, W. K., 1970, Biometrika, 57, 97
- Holt, J.W., Lim, Y. 2018, Phys. Lett. B, 784, 77
- Hong, B. et al. 2014, Euro Phys. J. A 50, 49
- Horowitz, C.J. et al. 2014, J. Phys. G **41**, 093001
- Keating, K.A., & Cherry S. 2009, Ecology 90:1971
- Kubis, S. 2004, Phys. Rev. C, 70, 065804
- Kubis, S. 2007, Phys. Rev. C, 76, 025801
- Kubis, S., & Kutschera, M. 2003, Nucl. Phys. A 720, 189
- Landry, P., & Essick, R. 2019, Phys. Rev. D 99, 084049
- Lattimer, J. M., & Prakash, M. 2000, Phys. Rep., 333, 121
- Lattimer, J. M., & Prakash, M. 2001, APJ, 550, 426
- Lattimer, J. M., & Prakash, M. 2007, Phys. Rep., 442, 109
- Lattimer, J.M. 2012, Annu. Rev. Nucl. Part. Sci. **62**, 485
- Lattimer, J. M., & Steiner, A. W. 2014, Eur. Phys. J. A, 50, 40
- Lee, C-H. 1996, Phys. Rep. 275, 255
- Li, B.A. & Steiner, A.W. 2006, Phys. Lett. B, 642, 436
- Li, B.A., Chen, L.W. & Ko, C.M. 2008, Phys. Rep. 464, 113
- Li, B. A., & Han, X. 2013, Phys. Lett. B, 727, 276
- Li, B. A., Ramos, À., Verde G., & Vidana, I. (Eds.) 2014, Eur. Phys. J. A, 50, 9
- Li, B. A. 2017, Nuclear Physics News, 27, 7
- Li, B.A., Krastev, P.G., Wen, D.H., & Zhang, N.B. 2019, Euro. Phys. J. A 55, 117
- Li, J.J., & Sedrakian, A. 2019, arXiv:1903.06057
- Lim, Y., & Holt, J. W. 2019, Phys. Rev. Lett. 121, 062701
- Lindblom, L. 2010, Phys. Rev. D **82**, 103011
- Lindblom, L. 2018, Phys. Rev. D **97**, 123019
- Malik, T. et al. 2018, Physical Review C 98, 035804
- Margueron, J., Hoffmann Casali, R., Gulminelli, F., 2018, Phys. Rev. C 97, 025805
- Margueron, J., Hoffmann Casali, R., Gulminelli, F., 2018, Phys. Rev. C 97, 025806
- Metropolis, N., Rosenbluth, A. W., Rosenbluth, M. N., & Teller, A. H., 1953, J. Chem. Phys. 21, 1087
- Miller, M. C., Chirenti, C., & Lamb, F. K. 2019, arXiv:1904.08907v1
- Muller, H., & Serot, B. 1995, Phys. Rev. C 52, 2072
- Nakazato, K. & Suzuki, H. 2019, Astrophysical Journal 878, 25.
- Negele, J. W., & Vautherin, D. 1973, Nucl. Phys. A, 207, 298
- Odrzywolek, A., & Kutschera, M. 2009, Acta. Phys. Polon. B40, 195
- Oertel, M., Hempel, M., Klähn, T., & Typel, S. 2017, Rev. Mod. Phys., 89, 015007
- Oppenheimer, J., & Volkoff, G. 1939, Phys. Rev., 55, 374
- Oyamatsu, K., & Iida, K. 2007, Phys. Rev. C, 75, 015801
- Özel, F., & Freire, P. 2016, Annual Reviews of Astronomy and Astrophysics, 54, 401
- Özel, F. et al. 2016, Astrophys. J. 820, 28
- Piekarewicz, J. 2010, J. Phys. G, 37, 064038
- Providência et al., C. 2019, Front. Astron. Space Sci., 26 March
- Raaijmakers, G., Riley, T. E., & Watts, A. L. 2018, Mon. Not. R. Astron. Soc. 478, 2177
- Raithe, C. A., Özel, F., & Psaltis, D. 2017, APJ, 844, 156
- Ray, P. S., et al., 2019, arXiv:1903.03035v2
- Ribes, P., Ramos, A., Tolos, L., Gonzalez-Boquera, C., & Centelles, M. 2019, arXiv:1907.08583
- Riley, T. E., Raaijmakers, G., & Watts, A. L. 2018, MNRAS, 478, 1093
- Russotto, P., et al., 2011, Phys. Lett. B **697**, 471
- Russotto, P., et al., 2016, Phys. Rev. C **94**, 034608
- Sahoo, H.S., et al. 2018, Phys. Rev. C **98**, 045801
- Shlomo, S., Kolomietz, V. M., & Colò G. 2006, Eur. Phys. J. A, 30, 23
- Sotani, H., Nakazato, K., Iida, K., & Oyamatsu, K. 2012, Phys. Rev. Lett., 108, 201101
- Steiner, A. W., Prakash, M., Lattimer, J. M., & Ellis, P. J. 2005, Phys. Rep., 410, 325
- Steiner, A. W., Lattimer, J. M., & Brown, E. F. 2010, APJ, 722, 33
- Sumiyoshi, K., & Toki, H. 1994, Astrophys. J. 422, 700.
- Tamii, A., von Neumann-Cosel, P., & Poltoratska, I. 2014, Euro. Phys. J. A 50, 28
- Tews, I., Lattimer, J. M., Ohnishi, A., & Kolomeitsev, E. E. 2017, APJ, 848, 105
- The 2015 U.S. Long Range Plan for Nuclear Science, Reaching for the Horizon, https://science.energy.gov/~media/npsac/pdf/2015LRP/2015_LRPNs_0
- The Nuclear Physics European Collaboration Committee (NuPECC) Long Range Plan 2017, Perspectives in Nuclear Physics, http://www.esf.org/fileadmin/user_upload/esf/Nupecc-LRP2017.pdf.
- Trautmann, W. & Wolter, H.H. 2012, Int. J. Mod. Phys. E **21**, 1230003
- Trautmann, W. 2019, AIP Conference Proceedings 2127, 020003
- Tsang et al., M.B. et al. 2012, Phys. Rev. C **86**, 015803
- Tolman, R. C. 1934, Proc. Natl. Acad. Sci. U.S.A., 20, 3
- Tong, H., Zhao, P.W., & Meng, J. 2019, arXiv:1903.05938v1.
- Trotta, R. 2017, arXiv:1701.01467

- Turkkan, N. & Pham-Gia T., J. Stat. Comput. Sim., 44, 243
- Vidaña, I. 2018, Proc. R. Soc. A **474**, 20180145
- Watts, A.L. et al, 2016, Rev. Mod. Phys., 88, 021001
- Watts, A.L. 2019, AIP Conference Proceedings 2127, 020008
- Wilson-Hodge, C.A. et al. 2016, Space Telescopes and Instrumentation 2016: Ultraviolet to Gamma Ray, Vol. 9905 of Proceedings of the SPIE, 99054Y
- Wu, X. H., & Shen, H. 2019, Phys. Rev. C 99, 065802
- Xiao, Z.G., Li, B.A., Chen, L.W., Yong, G.C., & Zhang, M. 2009, Phys. Rev. Lett. **102**, 062502
- Xu, H.S. et al. 2000, Phys. Rev. Lett. 85, 716
- Zhang, N. B., Cai, B. J., Li, B. A., Newton, W. G., & Xu, J. 2017, Nucl. Sci. Tech., 28, 181.
- Zhang, N. B., Li, B. A. & Xu, J. 2018, ApJ, 859, 90
- Zhang, N. B., & Li, B. A. 2019, Eur. Phys. J. A 55, 39
- Zhang, N. B., & Li, B. A. 2019, J. Phys. G. 46, 014002
- Zhang, N. B., & Li, B. A. 2019, APJ, 879, 99
- Zhang, S., Santangelo, A., Feroci, M., Xu, Y., et al. 2019, Science China Physics, Mechanics, and Astronomy 62, 29502
- Zhang, X., King, M. L., & Hyndman, R. J. 2006, Comput. Stat. Data. An. 50, 3009
- Zhou, Y., Chen, L.W., & Zhang, Z. 2019, Phys. Rev. D 99, 121301
- Zhu, Z.Y., et al. 2016, Phys. Rev. C 94, 045803